FOOD FRONTIERS Open Access

RESEARCH ARTICLE OPEN ACCESS

Decoding Chemical Profiles, Biological Functions, and Medicinal Properties of *Liquidambar orientalis* Extracts Through Molecular Modeling and Bioinformatic Methods

Mehmet Cengiz Baloglu[1,2] | Lutfiye Yildiz Ozer[3] | Buket Pirci[1] | Yasemin Celik Altunoglu[1] | Sanam Iram Soomro[4] | Gokhan Zengin[5] | Mehmet Veysi Cetiz[5,6] | Simone Carradori[7] | Zoltán Cziáky[8] | József Jekő[8]

[1]Plantomics Research Laboratory, Department of Genetics and Bioengineering, Faculty of Engineering and Architecture, Kastamonu University, Kastamonu, Türkiye | [2]SUNUM Nanotechnology Research Centre, Sabanci University, Istanbul, Türkiye | [3]College of Health and Life Sciences, Hamad Bin Khalifa University, Doha, Qatar | [4]Department of Community Health Sciences, Aga Khan University, Karachi, Pakistan | [5]Department of Biology, Science Faculty, Selcuk University, Konya, Türkiye | [6]Cetiz Lab. Sanlıurfa, Sanlıurfa, Türkiye | [7]Department of Pharmacy, "G. d'Annunzio" University of Chieti Pescara, Chieti, Italy | [8]Agricultural and Molecular Research and Service Institute, University of Nyíregyháza, Nyíregyháza, Hungary

Correspondence: Mehmet Cengiz Baloglu (mcbaloglu@kastamonu.edu.tr)

Received: 15 October 2024 | **Revised:** 21 December 2024 | **Accepted:** 2 January 2025

Funding: The authors received no specific funding for this work.

Keywords: antioxidant and antibacterial synergy | *Liquidambar orientalis* | molecular docking analysis | multi-targeted therapies | phytochemical profiling | therapeutic targets

ABSTRACT

Liquidambar orientalis, the Anatolian sweetgum tree, is a relict and endemic species in Southwestern Turkey, traditionally used for therapeutic purposes. Our study comprehensively evaluated the therapeutic potential of *L. orientalis* extracts from its aerial parts to maximize bioactive compound extraction using methanol, ethyl acetate, and water as solvents. The methanolic extract exhibited the highest phenolic (73.04 ± 3.94 mg gallic acid equivalent [GAE]/g) and flavonoid content (48.86 ± 0.76 mg rutin equivalent [RE]/g), demonstrating superior antioxidant activity in 2,2-diphenyl-1-picrylhydrazyl (DPPH) (256.61 ± 1.70 mg Trolox equivalent [TE]/g), 2,2′-azinobis-(3-ethylbenzothiazoline-6-sulfonic acid) (ABTS) (308.41 ± 3.14 mg TE/g), and cupric ion–reducing antioxidant capacity (CUPRAC) (411.13 ± 8.48 mg TE/g) assays. It also showed significant enzyme inhibition for acetylcholinesterase (4.43 ± 0.09 mg galanthamine equivalent [GALAE]/g), tyrosinase (149.16 ± 1.14 mg kojic acid equivalent [KAE]/g), amylase (0.93 ± 0.02 mmol acarbose equivalent [ACAE]/g), and glucosidase (1.60 ± 0.01 mmol ACAE/g), suggesting potential applications in neurodegenerative disease management, skincare, and diabetes treatment. Furthermore, methanol and water extracts displayed promising antimicrobial activity due to phenolic compounds such as chlorogenic acid and methyl-3-*O*-caffeoyl quinate. The methanolic extract exhibited potent anticancer effects against lung cancer (A549) cells, with significant reductions in cell viability and induction of autophagy. The aqueous extract showed remarkable efficacy against prostate cancer (PC3) cells, modulating apoptosis markers. Breast cancer cells (MDA-MB-231) exhibited differential responses, with ethyl acetate extract promoting apoptosis and water extract–enhancing autophagy. Furthermore, molecular docking and dynamics simulations provided additional evidence supporting the therapeutic potential of key phytochemicals from *L. orientalis*, particularly afzelin and epigallocatechin, against cancer-related targets and bacterial enzymes. Overall, this study fills a gap in understanding the enzyme

This is an open access article under the terms of the Creative Commons Attribution License, which permits use, distribution and reproduction in any medium, provided the original work is properly cited.

© 2025 The Author(s). *Food Frontiers* published by John Wiley & Sons Australia, Ltd and Nanchang University, Northwest University, Jiangsu University, Zhejiang University, Fujian Agriculture and Forestry University.

inhibitory and diverse anticancer effects of *L. orientalis* extracts, highlighting its potential multi-targeted therapeutic applications, particularly in cancer therapy.

1 | Introduction

The search for possible drug candidates capable of curing diseases, including diabetes, cancer, and hypertension, while minimizing side effects, has been a considerable challenge. Advances in drug discovery technology have led to the development of numerous therapeutic agents. Notably, several drugs derived from natural products, such as artemisinin from *Artemisia annua* and Taxol from *Taxus brevifolia*, have demonstrated remarkable efficacy in treating various diseases (Thomford et al. 2018).

Natural products, especially those extracted from plants, have been proven to be used for pharmaceutical purposes since ancient times due to their secondary metabolites, especially for phenolic compounds (Zengin et al. 2016; Ferrante et al. 2017). These phenolic substances, namely, phenols, flavonoids, tannins, coumarins, and lignans, are particularly known for their antioxidant properties that help neutralize free radicals and prevent oxidative stress. Oxidative stress is a key factor in the development of cancer, cardiovascular conditions, and neurodegenerative diseases (Perillo et al. 2020; Scheibmeir et al. 2005; Alkadi 2020; Kinghorn 1994). Given their wide range of beneficial effects, these plant-derived metabolites continue to be of significant interest for their potential health-promoting properties.

Liquidambar orientalis Mill. (*L. orientalis*), commonly referred to as the Anatolian sweetgum tree, is a deciduous and woody plant that belongs to the Hamamelidaceae family. It is a relict and endemic species, mainly spread to Southwestern Turkey, particularly in Mugla, Aydin, Burdur, Isparta, and the Greek island of Rhodes (Efe 2014). *L. orientalis* oil and other extracts have traditionally been used to treat various ailments, such as asthma, stroke, gastritis, ulcers, abdominal pain, and wounds (Gürdal and Kültür 2013; Ocsel et al. 2012). Previous studies have also demonstrated that *L. orientalis* oil has many therapeutic properties, including antioxidant, anti-inflammatory, antimicrobial, antifungal, anticancer, and anti-malarial due to its phenolic content (Avunduk and Kacar 2013; Nalbantsoy et al. 2016; Guzman 2014; Oskay and Sarı 2008; Sağdiç et al. 2005; Özbek and Bilek 2018; Baloglu et al. 2023).

Despite their widespread use in traditional medicine, the therapeutic potential of *L. orientalis* extracts has not been fully explored. Limited studies have reported on its biological properties. For example, Sarac and Şen (2014) showed the antioxidant, mutagenic, and antimutagenic activity of its ethanol extract due to the presence of protocatechuic acid, (−) epicatechin, and gallic acid (GA). Another group studied the antimicrobial activity of ethanol extract against methicillin-resistant *Staphylococcus aureus*, *Escherichia coli*, *Salmonella* Typhimurium, *Pseudomonas fluorescens*, *Proteus vulgaris*, *Serratia marcescens*, and *Staphylococcus epidermidis* (Oskay and Sarı 2008). Cetinkaya et al. (2022) reported that its leaf methanol extract, containing catechins, quercetin, chlorogenic acid, and kaempferol, had the highest cytotoxic effect through NF-κB and apoptotic pathways in colorectal cancer lines compared to *n*-hexane and ethyl acetate extracts.

However, there has been a notable lack of comprehensive research into the enzyme inhibitory activity of its extracts, as well as their effects on different cancer types. To address these gaps, the study employed Kyoto Encyclopedia of Genes and Genomes (KEGG) pathway enrichment, STRING network analysis, molecular docking, and simulation analyses. These techniques were utilized to examine the interactions of phytochemicals derived from *L. orientalis* with specific bacterial and cancer-related targets. By providing a comprehensive understanding of the gene networks, binding processes, and biological pathways that these drugs affect, these approaches have facilitated a more nuanced comprehension of the potential therapeutic benefits of these compounds (Yagi et al. 2024; Duran et al. 2024).

To investigate the broad pharmacological properties of *L. orientalis*, this study focuses on the phytochemical content, antimicrobial, antioxidant, enzyme inhibitory, and antitumor potential of its various solvent extracts (methanol, ethyl acetate, and water) derived from the aerial parts of the plant. Specifically, the study aims to elucidate the mechanism of antitumor activity by analyzing the expression levels of autophagy and apoptosis biomarkers. Moreover, the study's dual focus on both cancer and microbial inhibition is supported by the use of relevant antioxidant assays, such as DPPH (2,2-diphenyl-1-picrylhydrazyl), ABTS (2,2′-azinobis-(3-ethylbenzothiazoline-6-sulfonic acid)) assay, CUPRAC (cupric ion–reducing antioxidant capacity), FRAP (ferric-reducing antioxidant power), chelating ability, and phosphomolybdenum (PBD), which assess the plant extracts' ability to neutralize free radicals and reduce oxidative stress. These assays provide a foundation for understanding the potential of *L. orientalis* in cancer prevention and antimicrobial therapy. To the best of our knowledge, this is the first study to examine the enzyme-inhibitory activity of *L. orientalis* extracts and their effects on breast, lung, and prostate cancers. By combining molecular and biochemical techniques, this research aims to fill a critical gap in the understanding of this plant's therapeutic potential, ultimately contributing to naturally derived treatments for cancer and microbial infections.

2 | Materials and Methods

2.1 | Plant Materials and the Process of Extraction

L. orientalis Mill.'s aerial parts, including leaves and stem bark, were collected from the Muğla/Aksaz region of Turkey (GPS: 36°50′13″N, 28°22′57″E, 19 m).

Aerial parts of the plant were used to produce extracts in water, methanol, and ethyl acetate via the maceration technique. Ten

26438429, 2025, 3, Downloaded from https://adsn.onlinelibrary.wiley.com/doi/10.1002/ffd2.545 by Turkey Cochrane Evidence Aid, Wiley Online Library on [26/10/2026]. See the Terms and Conditions (https://onlinelibrary.wiley.com/terms-and-conditions) on Wiley Online Library for rules of use; OA articles are governed by the applicable Creative Commons License

grams of stem bark and leaves of 10 g were mixed and air-dried. They were softened in 200 mL of solvents at room temperature (25°C ± 1°C) for 24 h to create crude ethyl acetate and methanol extracts. The extracts were then concentrated under vacuum at 40°C using a rotary evaporator. On the other hand, in preparing crude water extract, 10 g of ground plant material was boiled in 200 mL distilled water for 30 min. Following this, the boiled solution was filtered and dried in a lyophilizer at −80°C for 48 h. The extracts were kept for additional examination at +4°C in the dark.

Ten grams of extracts were dissolved in 1 mL of solution to create the stock crude extracts. Following this, the crude extracts were centrifugated, and the supernatants were filtered through a 0.22 μm membrane filter. Subsequently, dilutions were prepared from the stock solution according to the required concentrations.

2.2 | Chromatographic Conditions

Liquid chromatography coupled with mass spectrometry (UHPLC/MS/MS) was used to analyze various extracts. The equipment used for this analysis was the Dionex Ultimate 3000RS UHPLC system, which was fitted with a mass spectrometer (Q-Exactive Orbitrap, Thermo, USA). Our previous publication included all analytical details (Zengin et al. 2018).

2.3 | Total Phenolic and Flavonoid Content Assay

Total phenolics and flavonoids were quantified according to Slinkard and Singleton's (1977) guidelines. The tests used rutin equivalent (RE) and GA as references; the outcomes were reported as RE and GA equivalents (GAE).

2.4 | Assays for In Vitro Antioxidant Capacity

Antioxidant testing was carried out using the procedures outlined by Grochowski et al. (2017). The results of the tests for DPPH, FRAP, CUPRAC, and ABTS radical scavenging were measured in milligrams of Trolox equivalents (TE) per gram of extract. The analysis for PBD revealed the antioxidant potential, which was measured in millimoles of TE per gram of extract. The milligrams of disodium edetate equivalents (EDTAE) per gram of extract was the unit of measurement for the metal chelating activity (MCA).

2.5 | Inhibitory Effects Against Some Key Enzymes

Enzyme inhibition tests were performed on the samples in accordance with known techniques (Grochowski et al. 2017). The inhibition of acetylcholinesterase (AChE) and butyrylcholinesterase (BChE) was measured in milligrams of galanthamine equivalents (GALAE) per gram of extract, whereas the inhibition of amylase and glucosidase was expressed in acarbose equivalents (ACAE) per gram of extract. In milligrams of kojic acid equivalents (KAE) per gram of extract, tyrosinase inhibition was measured.

2.6 | Determination of MIC and MBC

The antibacterial activity of *L. orientalis* Mill. stem bark and leaf extracts was assessed using 12 microorganisms, 6 of which were strains that were Gram-positive (*S. aureus* ATCC 25923, *Staphylococcus epidermis*, *Staphylococcus alpha haemolyticus*, *Enterococcus faecium*, *Listeria monocytogenes* ATCC 7644, and *Enterococcus durans*) and 6 of which were strains that were Gram-negative (*P. vulgaris*, *E. coli*, *Serratia marrescens*, *Pseudomonas aeruginosa*, *Salmonella kentucky*, *Enterobacter aerogenes* ATCC 13048). The Genetics and Bioengineering Department of Kastamonu University (Kastamonu, Türkiye) provided these bacterial strains.

2.7 | Cytotoxic Assessment

2.7.1 | Cell Culture Maintenance

A549, MDA-MB-231, and PC3 cancer cell lines were supplied by Kastamonu University (Biology Department, Türkiye), Boğaziçi University (Department of Molecular Biology and Genetics, Türkiye), and Selçuk University (Biochemistry Department, Türkiye), respectively. In an incubator with 5% carbon dioxide and 37°C, A549 and MDA-MB-231 cell lines were maintained in DMEM solution containing 10% FBS, 1% penicillin/streptomycin, 1% NEAA (non-essential amino acid), and 0.01 mg/mL human insulin. The PC3 cancer line was kept alive in DMEM solution with 1% NEAA, 10% FBS, and 1% penicillin/streptomycin. Following confluency, the cells were scraped with a cell scraper, treated for 5 min with a 0.25% trypsin–EDTA solution, and then rinsed with PBS. Centrifugation was used to gather the cells, with 5000 rpm for 5 min.

2.8 | MTT Assay and Calculation of IC_{50} Value

The cancer cell lines, A549 lung, MDA-MB-231 breast, and PC3 prostate (10^4 cells per well), were planted in 96-well plates and incubated for 24 h at 37°C in 5% CO_2. After that, the cells were treated with different concentrations of *L. orientalis* Mill. methanol, ethyl acetate, or water extracts, including 62.5, 125, 250, 500, and 1000 μg/mL, for 24 or 48 h. Following a replenishment of the media with DMEM containing 0.5% FBS and 0.5 μg/μL MTT, the cells were incubated for 4 h at 37°C in an incubator with 5% CO_2. After 5 min of 3% SDS mixture, the cells were exposed to 40 mM HCl/isopropanol for 15 min. A spectrophotometer set to 570 nm was used to measure the absorbance of the treated cells.

GraphPad Prism 7.0 (GraphPad Software, San Diego, California, USA) calculated the half maximum inhibitory concentration (IC_{50}) at 24 and 48 h.

2.9 | Gene Expression Level Assay

Plant extracts were applied to the cancer cells for 48 h at the IC_{50} dosage levels. After that, DNase treatment was applied to the extracted RNA using the GeneJET RNA purification Kit (Thermo Scientific, USA). Then, total RNAs were converted to cDNA using iScript cDNA Synthesis Kit (BioRad, USA). Table 1 indicates

26438429, 2025, 3, Downloaded from https://iadns.onlinelibrary.wiley.com/doi/10.1002/ffd2.545 by Turkey Cochrane Evidence Aid, Wiley Online Library on [26/10/2026]. See the Terms and Conditions (https://onlinelibrary.wiley.com/terms-and-conditions) on Wiley Online Library for rules of use; OA articles are governed by the applicable Creative Commons License

TABLE 1 | Primer sequences for real-time PCR.

Gene	Forward primer sequence (5′–3′)	Reverse primer sequence (5′–3′)
GAPDH	AACATGTAAACCATGTAGTTGAGGT	GGAAGGTGAAGGTCGGAGTC
LC3-II	GAGAAGCAGCTTCCTGTTCTGG	GTGTCCGTTCACCAACAGGAAG
Beclin-1	GGCTGAGAGACTGGATCAGG	CTGCGTCTGGGCATAACG
Bax	CCCGAGAGGTCTTTTTCCGAG	CCAGCCCATGATGGTTCTGAT
Bcl2	GGTGGGGTCATGTGTGTGG	CGGTTCAGGTACTCAGTCATCC

the primers that were used to measure the gene expression levels of autophagy and apoptotic indicators. SYBR Green Mix and Rotor Gene-Q (Qiagen, Germany) were used for real-time PCR analysis. The PCR amplification protocol involved 5 min of denaturation at 95°C, followed by 40 cycles of denaturation at 95°C for 10 min, annealing, and extension at 57°C for 30 s. The relative quantification of gene expressions was conducted with the comparative CT ($^{\Delta\Delta}$Ct) method (Livak and Schmittgen 2001).

2.10 | Screening of Potential Targets

The identification of therapeutic targets is a critical step in the development of novel drugs for use in medical research. In this regard, GeneCards and the Comparative Toxicogenomics Database (CTD) are valuable resources for identifying potential therapeutic targets in the context of cancer research. A search of the two databases for the term "breast, prostate, and lung cancer" yielded several associated genes. The databases TMCSD, PubChem, CTD, and SwissTarget were then used to identify the genes associated with the chemicals. To identify relevant targets associated with the effects of the drugs on breast, lung, and prostate cancer, common targets were identified using the Bioinformatics & Evolutionary Genomics web tool (https://bioinformatics.psb.ugent.be/webtools/Venn/) (Yagi et al. 2024; Zengin et al. 2024).

2.11 | Levels of Gene Expression for Essential Targets

The mRNA expression level and pathological staging association of the core target were validated using GEPIA. The threshold for $\log_2$FC is set at 1, whereas the threshold for p value is set at 0.01.

2.12 | KEGG Enrichment Analysis

To investigate the biological mechanisms and pathways associated with the important targets that *L. orientalis* might affect, a KEGG pathway enrichment analysis was performed. The Database for Annotation, Visualization, and Integrated Discovery (DAVID, V6.8, https://david.ncifcrf.gov/home.jsp) was used for the analysis (Huang, Sherman, and Lempicki 2009). The settings were configured as follows: Gene list was selected as list type, *Homo sapiens* was selected as species, and the official gene symbol was used as identification. A p value of less than 0.05 was set as the appropriate cutoff for statistical significance. R V4.3.3 software was used to generate the figure of analysis (Yagi et al. 2024; Zengin et al. 2024).

2.13 | Molecular Docking Protocol for Ligand–Protein Binding Analysis

The proteins and enzymes used in this study were obtained from the Protein Data Bank (PDB). The relevant information about standard enzymes (Yagi et al. 2024; Cusumano et al. 2024; Duran et al. 2024; Kurt-Celep et al. 2024), cancer-related proteins (Praveen et al. 2024; Zhang et al. 2024; Aboul-Soud et al. 2022; Gupta et al. 2024; Karahan et al. 2021), and antimicrobial proteins and enzymes (Saqallah et al. 2022) is given in Table S1. After retrieval of the structures, the meticulous elimination of co-crystallized ligands, cofactors, and water molecules was performed using BIOVIA Discovery Studio Visualizer V4.5. This step was necessary to prepare the proteins for docking experiments. The ligands were optimized using OpenBabel V3.1.1 after retrieval from the PubChem database (Zengin et al. 2024). MGL Tools version 1.5.6 was used to perform additional preparations of the protein and enzyme structures to ensure their suitability for subsequent analysis. The active sites in these proteins were identified using the CavitOmiX V1.0 plugin in PyMOL or literature-based inhibitor binding sites (Table S1) (Yagi et al. 2024; Duran et al. 2024). Re-docking was performed to confirm the accuracy of the initial docking results. The protein was redocked with the ligand, and the accuracy of the docking was evaluated by calculating the root mean square deviation (RMSD) values. The following formula was used to determine the RMSD, which is a metric of the average discrepancy between the atomic coordinates of the reference and target structures:

$$\mathrm{RMSD} = \sqrt{\frac{1}{N}\sum_{i=1}^{N}\left(r_i^{\mathrm{ref}} - r_i^{\mathrm{target}}\right)^2}$$

Protein–ligand interactions were further validated using BIOVIA Discovery Studio Visualizer V4.5, focusing on hydrogen bonds and other key interactions. Molecular docking was performed using AutoDock Vina V1.1.2, with grid boxes configured according to the technique described by Trott and Olson (2010).

2.14 | MM/PBSA Free Energy Calculations to Assess Ligand-Binding Affinity

In this study, the gmx_MMPBSA tool (https://valdes-tresanco-ms.github.io/gmx_MMPBSA/dev/getting-started/) was used to

26438429, 2025, 3, Downloaded from https://iadns.onlinelibrary.wiley.com/doi/10.1002/ff2.545 by Turkey Cochrane Evidence Aid, Wiley Online Library on [26/10/2026]. See the Terms and Conditions (https://onlinelibrary.wiley.com/terms-and-conditions) on Wiley Online Library for rules of use; OA articles are governed by the applicable Creative Commons License

calculate the free energy and evaluate the stability of the compounds. On the basis of the results of 10 ns molecular dynamics (MD) simulations, the compounds with the highest stability were selected for further analysis. Extended MD simulations (100 ns) were then performed on the selected compounds (Miller et al. 2012; Valdés-Tresanco et al. 2021).

2.15 | MD Simulation Setup for Ligand Stability and Flexibility

MD simulations were initiated using the CHARMM graphical user interface (GUI) platform, accessible at https://charmm-gui.org. The system setup was configured using the Solution Builder tool, originally developed by Jo et al. (2008). Proteins were parameterized using the CHARMM36m force field, following the methods described by Yagi et al. (2024) and Maier et al. (2015). A periodic boundary box containing TIP3P water molecules was used, maintaining a minimum distance of 10 Å between the protein and the box edges. Counterions were introduced to achieve neutralization and adjust the NaCl concentration to 0.15 M. The Verlet cutoff scheme was implemented for managing electrostatic and van der Waals interactions (VDWAALS), and bond lengths were constrained using the LINCS algorithm. Long-range electrostatics were calculated using the particle mesh Ewald (PME) method. Energy minimization was carried out using the steepest descent algorithm until the potential energy change was reduced below 1000 kJ/mol/nm. The system was equilibrated under NVT and NPT conditions at 303.3 K to ensure thermodynamic stability. Production simulations were performed using GROMACS 2024.2 over a duration of 100 ns (nstep = 50,000,000).

2.16 | Statistical Analysis

The statistical analysis was conducted using GraphPad Prism (version 9.0). First, the normality of all data was evaluated by the Shapiro–Wilk test. According to the results of the normality test, one-way ANOVA with Tukey post hoc test was conducted for comparisons among samples ($p < 0.05$).

3 | Results and Discussion

3.1 | Total Phenolics and Flavonoids

The *L. orientalis*, commonly known as sweetgum, has been studied for its rich phenolic and flavonoid contents. These phenolic and flavonoid compounds are known for their strong antioxidant activities, crucial in neutralizing free radicals, thereby reducing oxidative stress and preventing cellular damage. Engaging in this activity has been linked to a lower risk of developing long-term illnesses like cancer, heart disease, and neurological disorders (Rio et al. 2013). Studies have shown that the phenolic content in various plant extracts, including those of *L. orientalis*, can significantly inhibit radical formation and protect against DNA damage (Saraç and Şen 2014). However, the mixture allows for the extraction of unique active compounds from both parts, making our study unique and beneficial (Çetinkaya et al. 2022; Ulusoy, Ceylan, and Peker 2021).

In this study, the analysis of total phenolic content in three different solvents reveals distinct characteristics influenced by solvent properties, as shown in Table 2. The MeOH extract has a phenolic content of 73.04 ± 3.94 mg GAE/g, demonstrating methanol's effectiveness in disrupting plant cell walls and enhancing phenolic solubility through hydrogen bonding with phenolic hydroxyl groups. The water extract shows a phenolic content of 71.95 ± 0.12 mg GAE/g, highlighting water's ability to solubilize hydrophilic phenolic compounds and swell plant tissues, which increases extractability. The EA extract, with a phenolic content of 44.83 ± 2.10 mg GAE/g, illustrates ethyl acetate's limitations due to its lower dielectric constant and reduced efficiency in penetrating the plant matrix or solubilizing phenolic acids and glycosides. For total flavonoid content, the MeOH extract exhibits a flavonoid content of 48.86 ± 0.76 mg RE/g, indicating methanol's high efficiency in extracting flavonoid compounds. The water extract has a flavonoid content of 36.86 ± 0.10 mg RE/g, showing its capability to extract hydrophilic flavonoids and its role in swelling plant tissues to release flavonoids. The EA extract shows a flavonoid content of 10.58 ± 0.91 mg RE/g, reflecting ethyl acetate's lower efficiency in extracting flavonoid compounds. Previously, a wide range of analysis has been done on this plant in different ways, but research has analyzed different parts of *L. orientalis* separately. The bark chloroform extract exhibited the highest levels of phenolic (68.27 ± 0.30 mg/g) and flavonoid (34.10 ± 1.73 mg/g) contents, indicating significant antioxidant properties (Çetinkaya et al. 2022). Conversely, the leaf hexane extract had the lowest phenolic (25.08 ± 0.08 mg/g) and flavonoid (5.50 ± 1.71 mg/g) contents, suggesting weaker antioxidant potential. Other extracts, such as the leaf ethanol extract and fruit ethanol extract, showed substantial phenolic contents at 47.46 ± 0.11 mg/g and 62.41 ± 0.15 mg/g, respectively, with varying flavonoid contents of 10.06 ± 0.3 mg/g for the leaf ethanol extract and 9.73 ± 0.57 mg/g for the fruit ethanol extract. *L. orientalis* contains a good range of bioactive compounds, with the bark having higher individual priority. However, the mixture allows for the extraction of unique active compounds from both parts, making our study unique and beneficial (Çetinkaya et al. 2022; Ulusoy, Ceylan, and Peker 2021).

3.2 | Phytochemical Characterization

Utilizing analytical standards and relevant literature, the phytochemicals in the water, methanol, and ethyl acetate extracts were characterized using HPLC–ESI–MS in both negative and positive ion modes after the quantification of total phenolic and total flavonoids. Table 3 lists the 62 compounds in the negative ionization mode and the 7 compounds in the positive ionization mode that were found.

Previous studies demonstrated that the extraction method can vary the photochemical content of the plant extract. For example, the ethanol extract of *L. orientalis* Mill. contained protocatechuic acid, (−) epicatechin, GA, (+)-catechin (known for their antioxidant and anti-inflammatory properties), caffeic acid, ferulic acid, chlorogenic acid, *p*-coumaric acid, quercetin, kaempferol, and apigenin (Saraç and Şen 2014). However, quinic acid, quinalizarin, pyrocatechol, phloretin, phlorizin, hieracin, esculetin, genistin, methyl-gallate, naringenin, naringenin-7-*O*-

26438429, 2025, 3, Downloaded from https://iadns.onlinelibrary.wiley.com/doi/10.1002/ffd2.545 by Turkey Cochrane Evidence Aid, Wiley Online Library on [26/10/2026]. See the Terms and Conditions (https://onlinelibrary.wiley.com/terms-and-conditions) on Wiley Online Library for rules of use; OA articles are governed by the applicable Creative Commons License

TABLE 2 | Total phenolic and flavonoid contents of the examined extracts.

Extracts	Total phenolic content (mg GAE/g)	Total flavonoid content (mg RE/g)
EA	44.83 ± 2.10^{b}	10.58 ± 0.91^{c}
MeOH	73.04 ± 3.94^{a}	48.86 ± 0.76^{a}
Water	71.95 ± 0.12^{a}	36.86 ± 0.10^{b}

Note: Values expressed are means ± SD of three parallel measurements. Different letters indicate significant differences in the tested extracts ($p < 0.05$).
Abbreviations: GAE, gallic acid equivalent; RE, rutin equivalent.

glucoside, fisetin, and ellagic acid were all present in the methanol extract of its leaves (Çetinkaya et al. 2022).

In our study, a total of 76 phenolic compounds were identified from the extracts. The 10 identified compounds were identical to those found in the study by Sarac et al., with the exception of apigenin. Only two compounds, ellagic acid and naringenin, were identical to those identified in the study by Cetinkaya et al. Among the identified compounds in our study, GA, catechin, epigallocatechin, epigallocatechin-3-*O*-gallate, epicatechin, 4-coumaric acid, epicatechin-3-*O*-gallate, catechin-3-*O*-gallate, myricetin, quercetin, naringenin, kaempferol, alpha-linolenic acid, and linoleic acid were confirmed using standards.

As depicted in Table 3, phenolic acid found in the extracts were GA (compound 1), protocatechuic acid (3,4-dihydroxybenzoic acid) (compound 4), neochlorogenic acid (compound 5), dihydroxy-methoxybenzoic acid (compound 7), caffeic acid (compound 15), 3-*O*-(4-coumaroyl)quinic acid *cis* isomer (compound 8), 3-*O*-(4-coumaroyl)quinic acid (compound 11), 4-*O*-(4-coumaroyl)quinic acid *cis* isomer (compound 26), 4-*O*-(4-coumaroyl)quinic acid (compound 35), 4-coumaric acid (compound 36), *O*-coumaroyl-*O*-galloylhexose (compound 48), 3-*O*-feruloylquinic acid (compound 17), 4-*O*-feruloylquinic acid (compound 41), chryptochlorogenic acid (4-*O*-caffeoylquinic acid) (compound 25), methyl 3-*O*-caffeoylquinate (compound 28), ellagic acid (compound 53), 3-*O*-methylellagic acid (compound 61), 3,3′-Di-*O*-methylellagic acid (compound 66), and 3,3′,4-tri-*O*-methylellagic acid (compound 68). Flavan-3-ol monomers were (+)-catechin and its isomer (compounds 12, 39, 47, and 52), (−) epicatechin (compounds 31, 43, and 44), and, (+)-gallocatechin (3, 30, and 34), and (−)-epigallocatechin (13), epicatechin-3-*O*-gallate (29) and (+)-gallocatechin-3-*O*-gallate (21). Flavanols were myricetin and its derivatives (compounds 20, 49, 50, 51, and 54), quercetin and its derivatives (compound 55), Guaijaverin (compound 56), quercitrin (compound 64), kaempferol and its derivatives (compounds 67, 62, and 63).

3.3 | Antioxidant Activities

These identified phenolic compounds play a vital function as antioxidants by neutralizing free radicals, which can lead to oxidative stress and cellular damage, contributing to chronic diseases like cancer, cardiovascular diseases, and neurodegenerative disorders (Perillo et al. 2020; Scheibmeir et al. 2005; Alkadi 2020). The presence of these bioactive metabolites in plants is thus of significant interest for their potential health benefits.

The methanolic extract of *L. orientalis* leaves, known for its rich phenolic content, has demonstrated notable antioxidant activity in several studies (Saraç and Şen 2014; Çetinkaya et al. 2022; Ho et al. 2012; Okmen et al. 2014; Treml and Šmejkal 2016). This activity is largely attributed to the plant's ability to scavenge free radicals effectively. For instance, one study highlighted the methanolic extract's notable antioxidant protection, indicating its potential as a natural antioxidant source (Saravanakumar et al. 2021). Furthermore, DPPH scavenging activity is one of the tests that have been used to evaluate *L. orientalis*'s antioxidant activity. The antioxidant characteristics of the extracts obtained through supercritical fluid extraction were highlighted by their 90% DPPH scavenging activity (Saravanakumar et al. 2021).

These antioxidant properties not only provide significant health benefits but also offer potential applications in the cosmetic and food industries. By reducing oxidative stress, these extracts can help in preserving food products and enhancing the stability of cosmetic formulations (Baloglu et al. 2023; Özbek and Bilek 2018).

In our study, the MeOH extract shows the highest antioxidant capacity in the DPPH radical scavenging activity assay (256.61 ± 1.70 mg TE/g), indicating its effectiveness in neutralizing free radicals as shown in Table 4. The water extract also demonstrates considerable activity (189.44 ± 1.23 mg TE/g), whereas the EA extract shows significantly lower activity (62.29 ± 0.85 mg TE/g). Similarly, in the ABTS radical scavenging activity assay, the MeOH extract exhibits the highest activity (308.41 ± 3.14 mg TE/g), closely followed by the water extract (305.00 ± 11.24 mg TE/g), with the EA extract showing much lower activity (85.10 ± 3.15 mg TE/g). These findings highlight methanol's superior efficiency in extracting potent antioxidant compounds from the plant material. The CUPRAC assay, which measures the reduction capacity of the extracts, further supports the superior performance of the MeOH extract (411.13 ± 8.48 mg TE/g), with the water extract also showing high activity (401.76 ± 7.03 mg TE/g). The EA extract again exhibits the lowest activity in this assay (171.26 ± 2.89 mg TE/g). In the FRAP assay, the water extract demonstrates the highest reducing power (269.33 ± 4.99 mg TE/g), followed by the MeOH extract (237.28 ± 4.65 mg TE/g) and the EA extract (77.53 ± 2.17 mg TE/g).

In terms of chelating ability, which is important for binding and neutralizing metal ions, the water extract shows the highest capacity (17.78 ± 0.81 mg EDTAE/g), indicating its effectiveness in metal ion chelation. The MeOH extract also shows significant chelating ability (15.81 ± 0.75 mg EDTAE/g), whereas the EA extract has the lowest chelating ability (13.62 ± 0.66 mg EDTAE/g). The PBD assay results are relatively consistent across all extracts, with the EA extract showing slightly higher

26438429, 2025, 3, Downloaded from https://adsn.onlinelibrary.wiley.com/doi/10.1002/ffd2.545 by Turkey Cochrane Evidence Aid, Wiley Online Library on [26/10/2026]. See the Terms and Conditions (https://onlinelibrary.wiley.com/terms-and-conditions) on Wiley Online Library for rules of use; OA articles are governed by the applicable Creative Commons License

TABLE 3 | The characterization of the phenolic compound from *Liquidambar orientalis* Mill. extracts.

No.	Name	Formula	R_t	$[M+H]^+$	$[M-H]^-$	WE	MeOH	EA	Refs.
1[a]	Gallic acid (3,4,5-trihydroxybenzoic acid)	$C_7H_6O_5$	2.28		169.013	+	+	+	Saraç and Şen (2014), Çetinkaya et al. (2022)
2	Prodelphinidin B isomer 1	$C_{30}H_{26}O_{14}$	2.31		609.124	+	+	−	
3	Gallocatechin	$C_{15}H_{14}O_7$	4.56		305.066	+	+	+	
4	Protocatechuic acid (3,4-dihydroxybenzoic acid)	$C_7H_6O_4$	4.69		153.018	+	+	+	Saraç and Şen (2014), Çetinkaya et al. (2022)
5	Neochlorogenic acid (5-*O*-caffeoylquinic acid)	$C_{16}H_{18}O_9$	8.64	355.102		+	+	+	
6	Isostrictinin or isomer	$C_{27}H_{22}O_{18}$	9.40		633.072	+	−	−	
7	Dihydroxy-methoxybenzoic acid	$C_8H_8O_5$	11.22		183.029	+	+	+	
8	3-*O*-(4-Coumaroyl)quinic acid *cis* isomer	$C_{16}H_{18}O_8$	11.71		337.092	+	+	+	
9	Tellimagrandin I or isomer	$C_{34}H_{26}O_{22}$	11.98		785.083	+	−	−	
10	Prodelphinidin B isomer 2	$C_{30}H_{26}O_{14}$	12.35		609.124	+	+	−	
11	3-*O*-(4-Coumaroyl)quinic acid	$C_{16}H_{18}O8$	12.41		337.092	+	+	+	
12[a]	Catechin	$C_{15}H_{14}O_6$	13.28		289.071	+	+	+	Saraç and Şen (2014)
13[a]	Epigallocatechin	$C_{15}H_{14}O_7$	13.56		305.066	+	+	−	Çetinkaya et al. (2022)
14	Isostrictinin or isomer	$C_{27}H_{22}O_{18}$	13.68		633.072	+	+	−	
15	Caffeic acid	$C_9H_8O_4$	14.28		179.034	+	+	+	Saraç and Şen (2014)
16	Trimethoxyphenol isomer 1	$C_9H_{12}O_4$	14.34	185.081		+	+	+	
17	3-*O*-Feruloylquinic acid	$C_{17}H_{20}O_9$	14.43		367.102	+	+	+	
18	Trigalloylhexose isomer 1	$C_{27}H_{24}O_{18}$	14.46		635.088	+	+	−	
19	Hexosyl-hydroxycinnamate	$C_{15}H_{18}O_8$	14.53		325.092	+	+	+	
20	Ampelopsin (dihydromyricetin)	$C_{15}H_{12}O_8$	14.65		319.045	+	+	+	
21	Gallocatechin-*O*-gallate or epigallocatechin-*O*-gallate isomer 1	$C_{22}H_{18}O_{11}$	14.93		457.077	+	+	+	Çetinkaya et al. (2022)
22	Tellimagrandin I or isomer	$C_{34}H_{26}O_{22}$	15.05		785.083	+	+	−	
23	Prodelphinidin C isomer	$C_{30}H_{26}O_{13}$	15.10		593.129	−	+	−	
24	Digalloylhexose isomer 1	$C_{20}H_{20}O_{14}$	15.17		483.077	+	+	−	
25	Chryptochlorogenic acid (4-*O*-caffeoylquinic acid)	$C_{16}H_{18}O_9$	15.51	355.102		+	+	−	
26	4-*O*-(4-Coumaroyl)quinic acid *cis* isomer	$C_{16}H_{18}O_8$	15.52		337.092	+	+	+	
27	Digalloylhexose isomer 2	$C_{20}H_{20}O_{14}$	15.54		483.077	+	+	−	

(Continues)

26438429, 2025, 3, Downloaded from https://iadns.onlinelibrary.wiley.com/doi/10.1002/ffd.545 by Turkey Cochrane Evidence Aid, Wiley Online Library on [26/10/2026]. See the Terms and Conditions (https://onlinelibrary.wiley.com/terms-and-conditions) on Wiley Online Library for rules of use; OA articles are governed by the applicable Creative Commons License

TABLE 3 | (Continued)

No.	Name	Formula	R_t	$[M + H]^+$	$[M - H]^-$	WE	MeOH	EA	Refs.
28	Methyl 3-*O*-caffeoylquinate	$C_{17}H_{20}O_9$	15.73		367.102	−	+	−	
29[a]	Epigallocatechin-3-*O*-gallate (teatannin II)	$C_{22}H_{18}O_{11}$	16.36		457.077	+	+	−	Çetinkaya et al. (2022)
30	Gallocatechin-*O*-gallate or epigallocatechin-*O*-gallate isomer 2	$C_{22}H_{18}O_{11}$	16.56		457.077	+	+	+	Çetinkaya et al. (2022)
31[a]	Epicatechin	$C_{15}H_{14}O_6$	17.02		289.071	+	+	−	Saraç and Şen (2014)
33	Trigalloylhexose isomer 2	$C_{27}H_{24}O_{18}$	17.30		635.088	+	+	+	
34	Gallocatechin-*O*-gallate or epigallocatechin-*O*-gallate isomer 3	$C_{22}H_{18}O_{11}$	17.32		457.077	+	+	−	Çetinkaya et al. (2022)
35	4-*O*-(4-Coumaroyl)quinic acid	$C_{16}H_{18}O_8$	17.46		337.092	+	+	+	
36[a]	4-Coumaric acid	$C_9H_8O_3$	17.69		163.039	+	+	+	Saraç and Şen (2014), Çetinkaya et al. (2022)
37	Trimethoxyphenol isomer 2	$C_9H_{12}O_4$	17.9	185.081		+	−	+	
38	Tellimagrandin II or isomer	$C_{41}H_{30}O_{26}$	17.98		937.094	+	+	−	
39	Catechin-*O*-gallate or epicatechin-*O*-gallate isomer 1	$C_{22}H_{18}O_{10}$	18.14		441.082	+	+	−	
40	Isololiolide	$C_{11}H_{16}O_3$	18.19	197.117		+	+	+	
41	4-*O*-Feruloylquinic acid	$C_{17}H_{20}O_9$	18.47		367.102	+	+	−	
42	Casuarinin or isomer	$C_{41}H_{28}O_{26}$	18.67		935.079	−	+	−	
43	Catechin-*O*-gallate or epicatechin-*O*-gallate isomer 2	$C_{22}H_{18}O_{10}$	19.16		441.082	+	+	+	
44[a]	Epicatechin-3-*O*-gallate	$C_{22}H_{18}O_{10}$	19.33		441.082	+	+	−	
45	Tetragalloylhexose	$C_{34}H_28O_{22}$	19.37		787.090	+	+	+	
46	Loliolide	$C_{11}H_{16}O_3$	19.46			+	+	+	
47[a]	Catechin-3-*O*-gallate	$C_{22}H_{18}O_{10}$	20.35		441.082	+	+	−	
48	*O*-Coumaroyl-*O*-galloylhexose	$C_{22}H_{22}O_{12}$	20.52		477.103	+	+	−	
49	Myricetin-*O*-hexoside	$C_{21}H_{20}O_{13}$	20.86		479.082	+	+	+	
50	Myricitrin (Myricetin-3-*O*-rhamnoside)	$C_{21}H_{20}O_{12}$	21.91		463.087	+	+	+	
51	Myricetin-*O*-pentoside	$C_{20}H_{18}O_{12}$	22.07		449.072	+	+	+	
52	Catechin-*O*-gallate or epicatechin-*O*-gallate isomer 3	$C_{22}H_{18}O_{10}$	22.11		441.082	+	+	−	
53	Ellagic acid	$C_{14}H_6O_8$	23.36		300.99	+	+	+	Çetinkaya et al. (2022)
54[a]	Myricetin (3,3′,4′,5,5′,7-hexahydroxyflavone)	$C_{15}H_{10}O_8$	24.12		317.029	+	+	+	Çetinkaya et al. (2022)
55	Guaijaverin (Quercetin-3-*O*-arabinoside)	$C_{20}H_{18}O_{11}$	24.18		433.077	+	+	+	

(Continues)

26438429, 2025, 3, Downloaded from https://iadns.onlinelibrary.wiley.com/doi/10.1002/fft2.545 by Turkey Cochrane Evidence Aid, Wiley Online Library on [26/10/2026]. See the Terms and Conditions (https://onlinelibrary.wiley.com/terms-and-conditions) on Wiley Online Library for rules of use; OA articles are governed by the applicable Creative Commons License

TABLE 3 | (Continued)

No.	Name	Formula	R_t	$[M + H]^+$	$[M - H]^-$	WE	MeOH	EA	Refs.
56[a]	Quercitrin (Quercetin-3-*O*-rhamnoside)	$C_{21}H_{20}O_{11}$	24.39		447.092	+	+	+	
57	Myricetin-*O*-galloylrhamnoside isomer 1	$C_{28}H_{24}O_{16}$	24.42		615.098	+	+	+	
58	Myricetin-*O*-galloylrhamnoside isomer 2	$C_{28}H_{24}O_{16}$	24.61		615.098	+	+	+	
59	Myricetin-*O*-galloylrhamnoside isomer 3	$C_{28}H_{24}O_{16}$	24.95		615.098	+	+	+	
60	Abscisic acid	$C_{15}H_{20}O_4$	25.31		263.128	+	+	+	
61	3-*O*-Methylellagic acid	$C_{15}H_8O_8$	25.65		315.014	+	+	−	
62	Kaempferol-*O*-pentoside	$C_{20}H_{18}O_{10}$	25.98		417.082	+	+	+	
63	Afzelin (Kaempferol-3-*O*-rhamnoside)	$C_{21}H_{20}O_{10}$	26.35		431.097	+	+	+	
64[a]	Quercetin (3,3′,4′,5,7-pentahydroxyflavone)	$C_{15}H_{10}O_7$	26.93		301.034	+	+	+	Saraç and Şen (2014), Çetinkaya et al. (2022)
65[a]	Naringenin (4′,5,7-trihydroxyflavanone)	$C_{15}H_{12}O_5$	27.14		271.060	+	+	+	Çetinkaya et al. (2022)
66	3,3′-Di-*O*-methylellagic acid	$C_{16}H_{10}O_8$	27.81		329.029	+	+	−	
67[a]	Kaempferol (3,4’,5,7-tetrahydroxyflavone)	$C_{15}H_{10}O_6$	29.25		285.039	+	+	+	Saraç and Şen (2014), Çetinkaya et al. (2022)
68	3,3′,4-Tri-*O*-methylellagic acid	$C_{17}H_{12}O_8$	30.15		343.045	−	+	+	
69	Undecanedioic acid	$C_{11}H_{20}O_4$	30.81		215.128	−	−	+	
70	Pinocembrin (5,7-dihydroxyflavanone)	$C_{15}H_{12}O_4$	32.15		255.065	−	−	+	
71	Hydroxy-trimethoxyflavanone	$C_{18}H_{20}O_5$	33.12	317.138		+	+	+	
72	Hydroxyoctadecatrienoic acid	$C_{18}H_{30}O_3$	39.81		293.211	+	+	+	
73	Hydroxyoctadecadienoic acid	$C_{18}H_{32}O_3$	40.97		295.227	−	+	+	
74	Liquidambaric lactone or isomer	$C_{30}H_{44}O_4$	41.61	469.331		−	+	+	
75	α-Linolenic acid	$C_{18}H_{30}O_2$	44.71		277.216	−	+	+	
76	Dehydro(11,12) ursolic acid lactone or isomer	$C_{30}H_{46}O_3$	45.70	455.352		−	+	+	
76	Linoleic acid	$C_{18}H_{32}O_2$	45.71		279.232	−	+	+	

[a]Confirmed with an analytical standard.

26438429, 2025, 3, Downloaded from https://iadns.onlinelibrary.wiley.com/doi/10.1002/ffd2.545 by Turkey Cochrane Evidence Aid, Wiley Online Library on [26/10/2026]. See the Terms and Conditions (https://onlinelibrary.wiley.com/terms-and-conditions) on Wiley Online Library for rules of use; OA articles are governed by the applicable Creative Commons License

TABLE 4 | Antioxidant properties of the tested extracts.

Extracts	DPPH (mg TE/g)	ABTS (mg TE/g)	CUPRAC (mg TE/g)	FRAP (mg TE/g)	Chelating ability (mg EDTAE/g)	Phosphomolybdenum (mmol TE/g)
EA	62.29 ± 0.85^{c}	85.10 ± 3.15^{c}	171.26 ± 2.89^{c}	77.53 ± 2.17^{c}	13.62 ± 0.66^{c}	2.95 ± 0.19^{a}
MeOH	256.61 ± 1.70^{a}	308.41 ± 3.14^{a}	411.13 ± 8.48^{a}	237.28 ± 4.65^{b}	15.81 ± 0.75^{b}	2.77 ± 0.06^{c}
Water	189.44 ± 1.23^{b}	305.00 ± 11.24^{ab}	401.76 ± 7.03^{b}	269.33 ± 4.99^{a}	17.78 ± 0.81^{a}	2.88 ± 0.10^{b}

Note: Values expressed are means ± SD of three parallel measurements. Different letters indicate significant differences in the tested extracts ($p < 0.05$).
Abbreviations: ABTS, 2,2′-azinobis-(3-ethylbenzothiazoline-6-sulfonic acid); CUPRAC, cupric ion–reducing antioxidant capacity; DPPH, 2,2-diphenyl-1-picrylhydrazyl; EDTAE, EDTA equivalent; FRAP, ferric-reducing antioxidant power; na, not active; TE, Trolox equivalent.

activity (2.95 ± 0.19 mmol TE/g) compared to the MeOH (2.77 ± 0.06 mmol TE/g) and water (2.88 ± 0.10 mmol TE/g) extracts.

The total phenolic and flavonoid contents in the different extracts show correlation with DPPH, ABTS, and CUPRAC assays. The MeOH extract, which contained the highest levels of phenolic and flavonoid compounds, exhibited the strongest antioxidant activities across all assays, confirming the crucial role of these compounds in the antioxidant properties of *L. orientalis*. However, the correlation between the ABTS and hydroxyl radical scavenging activity was found to be nonsignificant, which could be due to differences in the solubility and chemical interactions of specific phenolic compounds in the different solvents. For instance, methanol may preferentially dissolve certain phenolic compounds that are more effective in scavenging DPPH and ABTS radicals, whereas water may better solvent compounds that contribute to reducing power (FRAP) and metal ion chelation. These variations in the oxidant activity emphasize the importance of solvent type and antioxidant assays.

The high antioxidant and chelating activities of the methanol and water extracts suggest that these extracts are particularly rich in bioactive compounds, which can provide significant health benefits. Several searches have been done on this plant on individual parts but not all parts; therefore, our study has novelty over them. The antioxidant activity of *L. orientalis* has been extensively evaluated in previous studies using various assays, yielding significant results. For instance, the DPPH assay demonstrated IC_{50} values ranging from 20 to 50 μg/mL, indicating strong free radical scavenging activity (Saraç and Şen 2014). Similarly, the ABTS assay, renowned for its sensitivity, reported TEAC values between 0.5 and 2.0 mmol Trolox/g extract, further highlighting the plant's remarkable antioxidant capacity (Baloglu et al. 2023). The CUPRAC assay, which measures reducing power, reported values around 1.0–3.0 mmol Trolox/g extract, demonstrating notable antioxidant potential (Özyürek, Güçlü, and Apak 2011). Additionally, the FRAP assay showed values ranging from 0.5 to 1.5 mmol Fe(II)/g extract, confirming the plant's ability to reduce ferric ions. Lastly, *L. orientalis* exhibited moderate chelating ability, with 40%–60% inhibition at 1–2 mg/mL, and high total antioxidant capacity as indicated by significant absorbance values in the PBD assay (Ulusoy, Ceylan, and Peker 2021; Zengin and Aktumsek 2014).

In conclusion, the study provides a detailed analysis of the antioxidant potential of *L. orientalis* extracts, demonstrating that the methanol and water extracts are particularly rich in high content of phenolic compounds and flavonoids, particularly GA, protocatechuic acid, gallocatechin, epicatechin, and caffeic acid (Kim et al. 2019; Plumb et al. 2002; Yagi et al. 2024). These compounds show significant antioxidant, chelating, and free radical scavenging activities, which are essential for preventing oxidative stress-related diseases. The correlation between phenolic and flavonoid content and antioxidant activity underscores the importance of these bioactive compounds in the therapeutic potential of *L. orientalis*. This study contributes to a more comprehensive understanding of the bioactivity of *L. orientalis*, providing valuable insights for potential applications in health, food, and cosmetic industries.

26438429, 2025, 3, Downloaded from https://adsn.onlinelibrary.wiley.com/doi/10.1002/ffd2.545 by Turkey Cochrane Evidence Aid, Wiley Online Library on [26/10/2026]. See the Terms and Conditions (https://onlinelibrary.wiley.com/terms-and-conditions) on Wiley Online Library for rules of use; OA articles are governed by the applicable Creative Commons License

3.4 | Enzyme Inhibitory Properties

Because of its possible medical uses, *L. orientalis* extracts' inhibitory effects on enzymes like AChE, BChE, tyrosinase, amylase, and glucosidase are of significant interest. For instance, the inhibition of AChE and BChE is relevant in treating neurodegenerative diseases like Alzheimer's, as these enzymes break down acetylcholine, a neurotransmitter involved in memory and learning. Tyrosinase inhibitors are valuable in cosmetics for skin-lightening and anti-browning in food processing. Amylase and glucosidase inhibitors are important for managing diabetes by slowing the breakdown and absorption of carbohydrates, thereby regulating blood sugar levels (Rahman et al. 2021; Saravanakumar et al. 2021; Zengin and Aktumsek 2014).

Among the extracts, the MeOH extract shows the highest AChE inhibition at 4.43 ± 0.09 mg GALAE/g, indicating its potential effectiveness for enhancing cholinergic neurotransmission, which is beneficial in treating conditions like Alzheimer's disease. The EA extract also shows notable AChE inhibition (2.89 ± 0.13 mg GALAE/g), whereas the water extract has the lowest AChE inhibition (2.07 ± 0.06 mg GALAE/g) (Table 5). For BChE inhibition, the EA extract leads with 3.00 ± 0.46 mg GALAE/g, followed by the MeOH extract (2.72 ± 0.36 mg GALAE/g), with no available data for the water extract.

Regarding tyrosinase inhibition, the MeOH extract again shows the highest activity (149.16 ± 1.14 mg KAE/g), which can be useful in skin-lightening and anti-browning applications in the food industry. The EA extract shows significant tyrosinase inhibition (131.56 ± 1.78 mg KAE/g), whereas the water extract has the lowest (91.64 ± 0.75 mg KAE/g), as shown in Table 5.

The MeOH extract also exhibits the highest amylase inhibition (0.93 ± 0.02 mmol ACAE/g), which can aid in managing diabetes by slowing carbohydrate digestion. The EA extract shows considerable amylase inhibition (0.87 ± 0.02 mmol ACAE/g), whereas the water extract shows minimal inhibition (0.12 ± 0.01 mmol ACAE/g). Finally, in glucosidase inhibition, the MeOH extract leads again with 1.60 ± 0.01 mmol ACAE/g, followed by similar levels in the EA (1.55 ± 0.04 mmol ACAE/g) and water extracts (1.54 ± 0.08 mmol ACAE/g).

These findings suggest that its methanol extract is particularly effective in extracting bioactive compounds with various health benefits, including antioxidant, anti-diabetic, and neuroprotective properties. Previous research has largely emphasized the enzyme-inhibitory properties of *L. orientalis* essential oil and the antioxidant and phenolic composition of its extracts; however, this study is the first to provide a comprehensive evaluation of the enzyme-inhibitory effects of its extracts. This novel investigation underscores the therapeutic potential of these extracts, particularly as promising candidates for managing neurodegenerative diseases and metabolic disorders.

3.5 | Antimicrobial Activity

With the overuse or misuse of antibiotics, emerging antibiotic resistance has become one of the significant health problems. This has underscored the importance of finding alternative

TABLE 5 | Enzyme inhibitory properties of the tested extracts.

Extracts	AChE inhibition (mg GALAE/g)	BChE inhibition (mg GALAE/g)	Tyrosinase inhibition (mg KAE/g)	Amylase inhibition (mmol ACAE/g)	Glucosidase inhibition (mmol ACAE/g)
EA	2.89 ± 0.13^{b}	3.00 ± 0.46^{a}	131.56 ± 1.78^{b}	0.87 ± 0.02^{ab}	1.55 ± 0.04^{b}
MeOH	4.43 ± 0.09^{a}	2.72 ± 0.36^{b}	149.16 ± 1.14^{a}	0.93 ± 0.02^{a}	1.60 ± 0.01^{a}
Water	2.07 ± 0.06^{c}	na	91.64 ± 0.75^{c}	0.12 ± 0.01^{c}	1.54 ± 0.08^{b}

Note: Values expressed are means ± SD of three parallel measurements. Different letters indicate significant differences in the tested extracts ($p < 0.05$).
Abbreviations: ACAE, acarbose equivalent; GALAE, galanthamine equivalent; KAE, kojic acid equivalent; na, not active.

26438429, 2025, 3, Downloaded from https://iadns.onlinelibrary.wiley.com/doi/10.1002/ffd2.545 by Turkey Cochrane Evidence Aid, Wiley Online Library on [26/10/2026]. See the Terms and Conditions (https://onlinelibrary.wiley.com/terms-and-conditions) on Wiley Online Library for rules of use; OA articles are governed by the applicable Creative Commons License

drugs, especially those derived from natural sources. In this context, plant-based molecules have become key candidates for developing new antimicrobial agents.

In our study, the antimicrobial activity of *L. orientalis* extract was evaluated against 12 bacterial strains by MBC and MIC methods. All the extracts demonstrated effectiveness against *E. aerogenes*. As indicated in Table 6, only methanol extract showed antimicrobial effect against *S. kentucky*, *S. epidermis*, and *E. faecium*.

Extracts made of water and methanol demonstrated efficacy against *E. durans* and *S. aureus*. However, the extracts did not show activity against *S. alpha hemolyticus*, *P. vulgaris*, *P. aeruginosa*, and *S. marcescens*. Previous research has indicated that compounds such as kaempferol, quercetin, and chlorogenic acid were not effective against *P. aeruginosa* (Adamczak, Ożarowski, and Karpiński 2020).

When evaluating the antibacterial efficacy of extracts against various bacterial strains, the most successful extracts were ethyl acetate, water, and methanol extracts, in that order. Gram-positive bacteria were more susceptible to the effects of methanol than Gram-negative bacteria. These extracts have antibacterial properties because they include bioactive substances, such as isomers of prodelphinidin, phenolic acids, and derivatives of chlorogenic acid. Specifically, chlorogenic acid was found in both water and methanol extracts, whereas methyl 3-caffeoylquinate was only present in the methanol extract. Previous studies have shown that chlorogenic acid and its derivatives possess antioxidant and antibacterial properties, disrupting bacterial membranes and inhibiting the growth of pathogens like *Bacillus cereus*, *E. coli*, *S. aureus*, and *Enterococcus faecalis* (Lou et al. 2011; Fiamegos et al. 2011; Nunes et al. 2016; Duangjai et al. 2016).

Okmen et al. (2014) reported that the methanol extract of *L. orientalis* impeded the growth of eight bacterial strains, including *S. aureus*, *E. faecium*, *L. monocytogenes*, and *E. coli*, at concentrations ranging from 1624 to 3250 μg/mL. This higher concentration used in their study might explain the discrepancy with our results, where effective concentrations were lower.

Overall, our findings suggest that *L. orientalis* extracts, particularly methanol and water extracts, hold promise as potential natural antimicrobial agents, offering a valuable alternative to traditional antibiotics.

3.6 | Anticancer Effect

Cancer, the second main reason for death worldwide, has attracted many researchers to find anticancer therapeutic agents without any side effects. For this reason, natural products, especially plant-derived, have emerged as promising therapeutic agents. Despite their potential, their perspective effect has not been thoroughly investigated due to their complex compositions, containing phenols, ketones, alcohol, and terpene compounds. These compounds can alter cell growth, cycle, and death (Bayala et al. 2014).

In this study, the cytotoxic properties of *L. orientalis* Mill. extract, methanol, and water were examined against A549, MDA-MB-231, and PC3 cancer cells. The extracts were tested at five different concentrations: 62.5, 125, 250, 500, and 1000 μg/mL, with incubation times of 24 or 48 h, using an MTT-based cytotoxicity assay.

The results, shown in Figures 1–3, demonstrated a dose- and time-dependent reduction in cancer cell survival rates. For the MDA-MB-231 breast cancer line, methanol extracts were the most effective after 24 h, whereas water extracts showed superior efficacy at 48 h. In the A549 lung cancer line, methanol extracts were effective at both 24 and 48 h. For the PC3 prostate cancer line, water extracts were most effective at both time points, followed closely by methanol extracts. The ethyl acetate extract was the least effective, likely due to its lower phenolic content, including prodelphinidin, cryptochlorogenic acid, catechin-*o*-gallate, casuarinin, and epicatechin-3-*o*-gallate, which are known for their significant cytotoxic effects.

On the basis of the cell viability assay, the IC_{50} values of the plant extracts on cancer cells were also ascertained. Methanol and water extracts had the lowest IC_{50} values after 24 h for the A549 and MDA-MB-231 lines. For the PC3 line, water extracts had the lowest IC_{50} value, followed by methanol extracts. With an IC_{50} value of 879 μg/mL, the methanol extract showed the most inhibitory impact on PC3 prostate cancer cells. The IC_{50} value for ethyl acetate could not be determined as it exceeded the highest concentration tested (1000 μg/mL).

Because chlorogenic acid and its derivatives are known to cause apoptosis and prevent metastasis, the presence of these compounds accounts for the methanol extract's potency (Çetinkaya et al. 2022). Additionally, the leaf methanol extract of *L. orientalis*, which contains high levels of flavonoids, showed significant cytotoxic activity against colorectal cancer lines.

The previous studies indicated that cinnamic acid (Pontiki et al. 2014), caffeic acid (Rzepecka-Stojko et al. 2015), and GA were effective against MDA MB 213 cancer cells. For A549 cancer cells, cinnamic acid (Tsai et al. 2013), caffeic acid (Tsai et al. 2013), chlorogenic acid, ferulic acid phenyl ester, and *p*-coumaric acid (Chang and Shen 2014) show anticancer activity. Ferulic acid (Eroğlu et al. 2015) was also reported as having an efficient cytotoxic effect on PC3 prostate cancer cells.

The anticancer mechanism of *L. orientalis* extracts in different cancer cells was further studied through the gene expression level of autophagy and apoptosis markers. The phenolic component-induced cell death can occur through different mechanisms: apoptosis, autophagy, and necrosis (Benvenuto et al. 2020). DNA and cell membranes breaking during apoptosis, a type of planned cell death, are indicative of the process; pro-apoptotic markers are Bax, and anti-apoptotic markers are Bcl-2. Autophagy maintains cellular homeostasis through a highly regulated process involving autophagy-related proteins. Key autophagy marker genes include Beclin I, which is involved in the nucleation step, and LC3 II, which is associated with the autophagosome.

L. orientalis treatment might induce autophagy or apoptosis on MDA MB 231, A549, and PC3 cancer lines. According to

26438429, 2025, 3, Downloaded from https://adsn.onlinelibrary.wiley.com/doi/10.1002/ffd2.545 by Turkey Cochrane Evidence Aid, Wiley Online Library on [26/10/2026]. See the Terms and Conditions (https://onlinelibrary.wiley.com/terms-and-conditions) on Wiley Online Library for rules of use; OA articles are governed by the applicable Creative Commons License

TABLE 6 | Antimicrobial activity of *Liquidambar orientalis* Mill. water, methanol, and ethyl acetate extracts against six Gram-positive and six Gram-negative bacteria strains.

	Water		Methanol		Ethyl acetate		Standard drug
Test strains	**MIC**	**MBC**	**MIC**	**MBC**	**MIC**	**MBC**	**Levofloxacin**
Gram-positive bacteria							
Staphylococcus aureus ATCC 25923	250	1000	500	500	500	—	31.2
Staphylococcus epidermis	500	—	500	500	1000	—	62.5
Staphylococcus alpha haemolyticus	500	—	—	—	—	—	62.5
Enterococcus faecium	500	—	500	1000	1000	—	15.6
Listeria monocytogenes ATCC 7644	500	1000	—	—	1000	—	15.6
Enterococcus durans	250	1000	500	1000	1000	—	15.6
Gram-negative bacteria							
Proteus vulgaris	500	—	500	—	—	—	15.6
Escherichia coli	500	1000	1000	—	500	1000	15.6
Serratia marrescens	500	—	1000	—	1000	—	31.2
Pseudomonas aeruginosa	500	—	—	—	1000	—	15.6
Salmonella kentucky	1000	—	500	1000	—	—	NT
Enterobacter aerogenes ATCC 13048	500	1000	500	1000	1000	1000	NT

Note: Values expressed are means of three measurements.

Abbreviations: MBC, minimum bactericidal concentration (μg/mL); MIC, minimum inhibitory concentration (μg/mL).

26438429, 2025, 3, Downloaded from https://iadns.onlinelibrary.wiley.com/doi/10.1002/fft2.545 by Turkey Cochrane Evidence Aid, Wiley Online Library on [26/10/2026]. See the Terms and Conditions (https://onlinelibrary.wiley.com/terms-and-conditions) on Wiley Online Library for rules of use; OA articles are governed by the applicable Creative Commons License

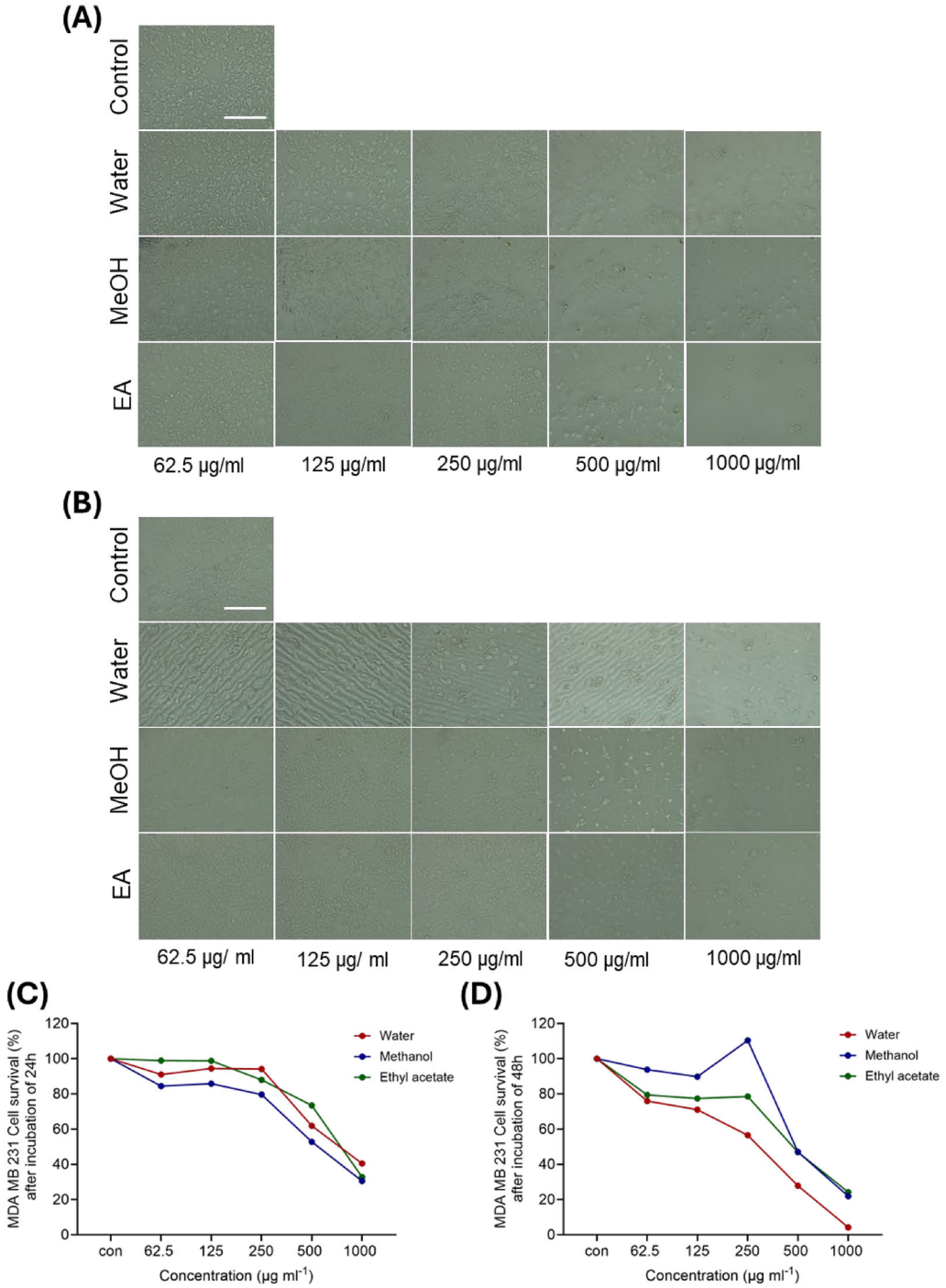


FIGURE 1 | MDA-MB-231 breast cancer cell (A and C) after incubation of 24 h and (B and D) after incubation of 48 h. Values expressed are means of eight measurements.

Figure 4, in the MDA-MB-231 line, treatment with ethyl acetate extract increased Bax gene expression, indicating an apoptotic pathway while reducing Beclin expression. Conversely, water extract treatment decreased Bax expression and increased Bcl-2 levels, potentially due to the presence of pinocembrin. Zhu et al. (2021) reported that pinocembrin, found in eucalyptus and other plants, inhibits proliferation and induces apoptosis by downregulating phosphorylated AKT and PI3K in MDA MB 231 and MCF7 cancer cells.

For A549 lung cancer cells, water and methanol extracts increased LC3-II expression, suggesting enhanced autophagy, while reducing Bax and Beclin expression, as shown in Figure 4. All extracts induced LC3-II expression and decreased Bax and Beclin levels in PC3 prostate cancer cells. This effect may be attributed to phenolic compounds such as catechin and epigallocatechin-3-gallate. Previous research has shown that epigallocatechin-3-gallate from green tea (Sonoda et al. 2014), curcumin (Liu et al. 2017), ursolic, and oleanolic acid (Castrejón-Jiménez et al. 2019) compounds can

26438429, 2025, 3, Downloaded from https://iadns.onlinelibrary.wiley.com/doi/10.1002/ffd2.545 by Turkey Cochrane Evidence Aid, Wiley Online Library on [26/10/2026]. See the Terms and Conditions (https://onlinelibrary.wiley.com/terms-and-conditions) on Wiley Online Library for rules of use; OA articles are governed by the applicable Creative Commons License

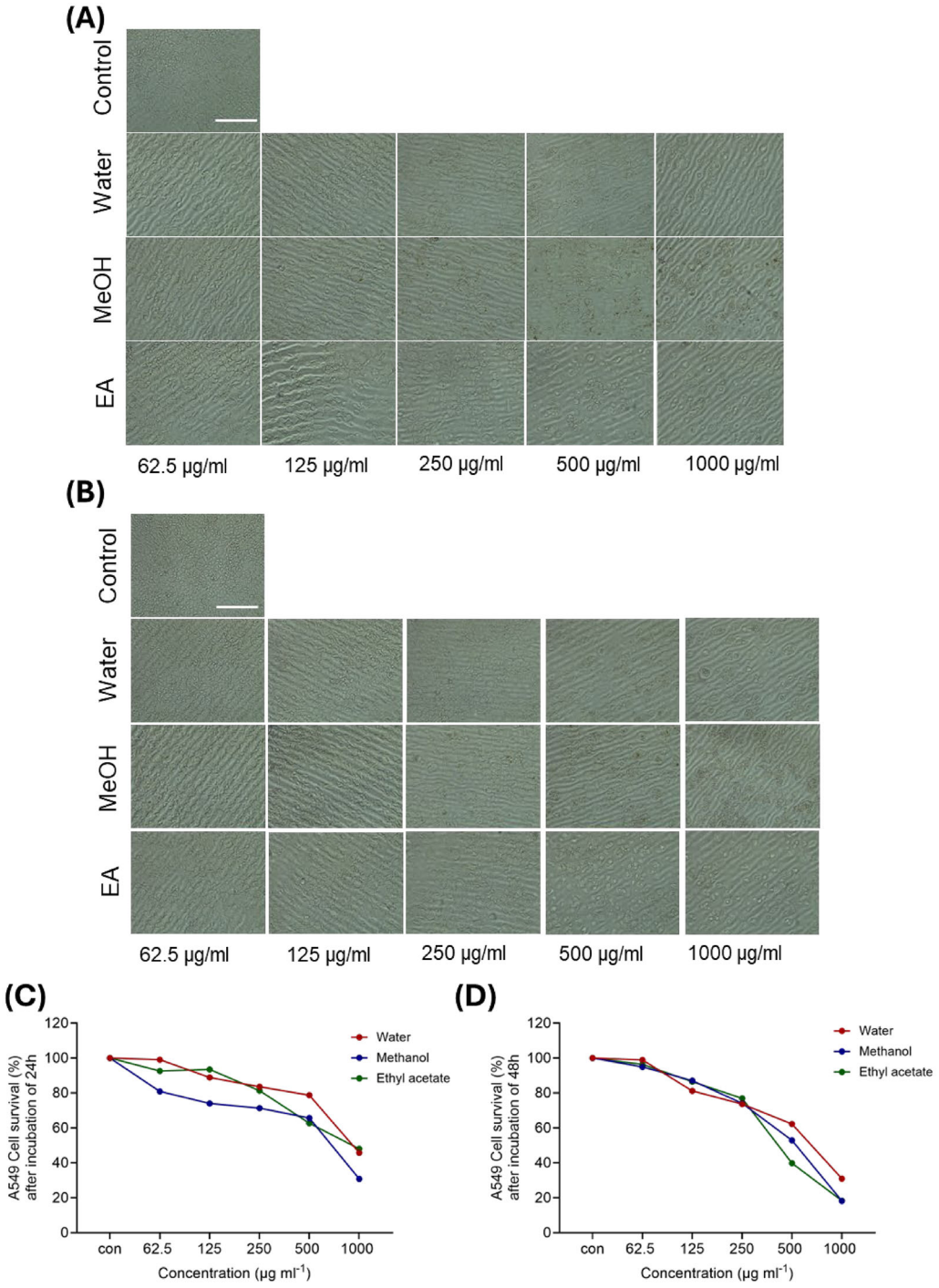


FIGURE 2 | A549 lung cancer line (A and C) after incubation of 24 h and (B and D) after incubation of 48 h. Values expressed are means of eight measurements.

modulate autophagy and apoptosis in A549 and PC3 cells through various mechanisms.

In summary, this study highlights the therapeutic potential of *L. orientalis* extracts in cancer treatment. The unique combination of bioactive compounds in these extracts, including chlorogenic acid and flavonoids, offers promising avenues for further exploration in developing effective natural anticancer agents. However, the effects of these phenolic compounds cannot fully show the mechanism of the autophagy pathway. For this reason, phenolic compounds found in *L. orientalis* extracts on autophagy should be exploited further.

3.7 | The Relationship Between Active Compounds of *L. orientalis* and Genes in Cancer

Following the identification of genes associated with phytochemicals derived from *L. orientalis*, a Venn diagram was used to investigate the relationships between these genes and those

26438429, 2025, 3, Downloaded from https://iadns.onlinelibrary.wiley.com/doi/10.1002/ffd2.545 by Turkey Cochrane Evidence Aid, Wiley Online Library on [26/10/2026]. See the Terms and Conditions (https://onlinelibrary.wiley.com/terms-and-conditions) on Wiley Online Library for rules of use; OA articles are governed by the applicable Creative Commons License

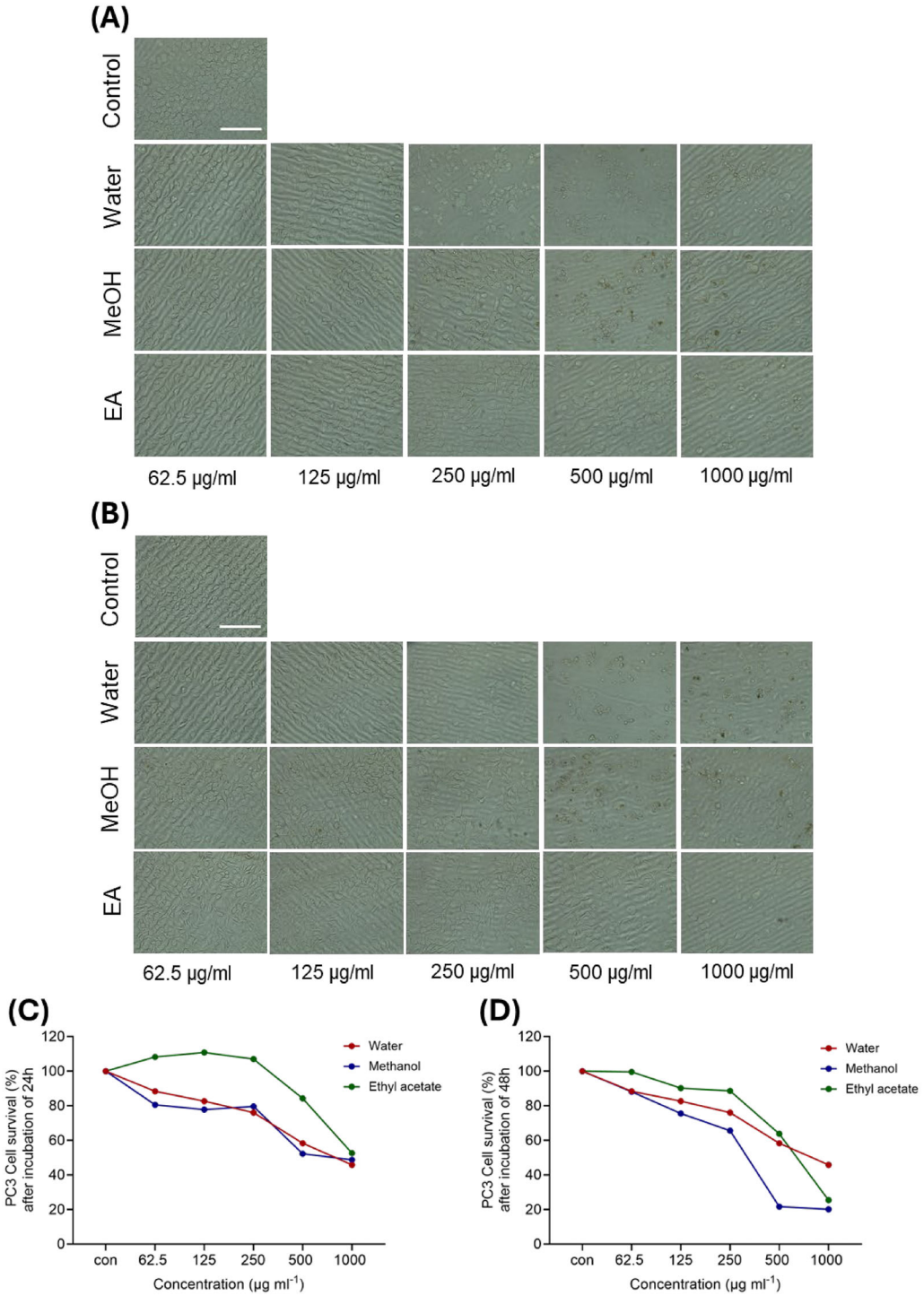


FIGURE 3 | PC3 prostate cancer line (A and C) after incubation of 24 h and (B and D) after incubation of 48 h. Values expressed are means of eight measurements.

specific to lung, prostate, and breast cancer. A comparison was made between the 3697 genes associated with this plant compound and the 152 genes associated with breast cancer, the 38 genes associated with prostate cancer, and the 591 genes associated with lung cancer retrieved from the CTD and GeneCards databases. The Venn diagram (Figure 5) illustrates the overlap between the gene sets of these phytochemicals and the selected cancer types. This shows which genes are shared between the phytochemicals and the cancer types. In this analysis, based on the number of edges, catechin, ellagic acid, and myricetin stand out prominently.

This investigation illuminated the possible biological roles of overlapping genes and their applicability as therapeutic targets in cancer therapy. These results establish a foundation for future investigations in this field and advance our understanding of the molecular pathways driving cancer biology. A gene interaction network comprising 152 nodes and 3981 edges was identified

26438429, 2025, 3, Downloaded from https://iadns.onlinelibrary.wiley.com/doi/10.1002/ffd2.545 by Turkey Cochrane Evidence Aid, Wiley Online Library on [26/10/2026]. See the Terms and Conditions (https://onlinelibrary.wiley.com/terms-and-conditions) on Wiley Online Library for rules of use; OA articles are governed by the applicable Creative Commons License

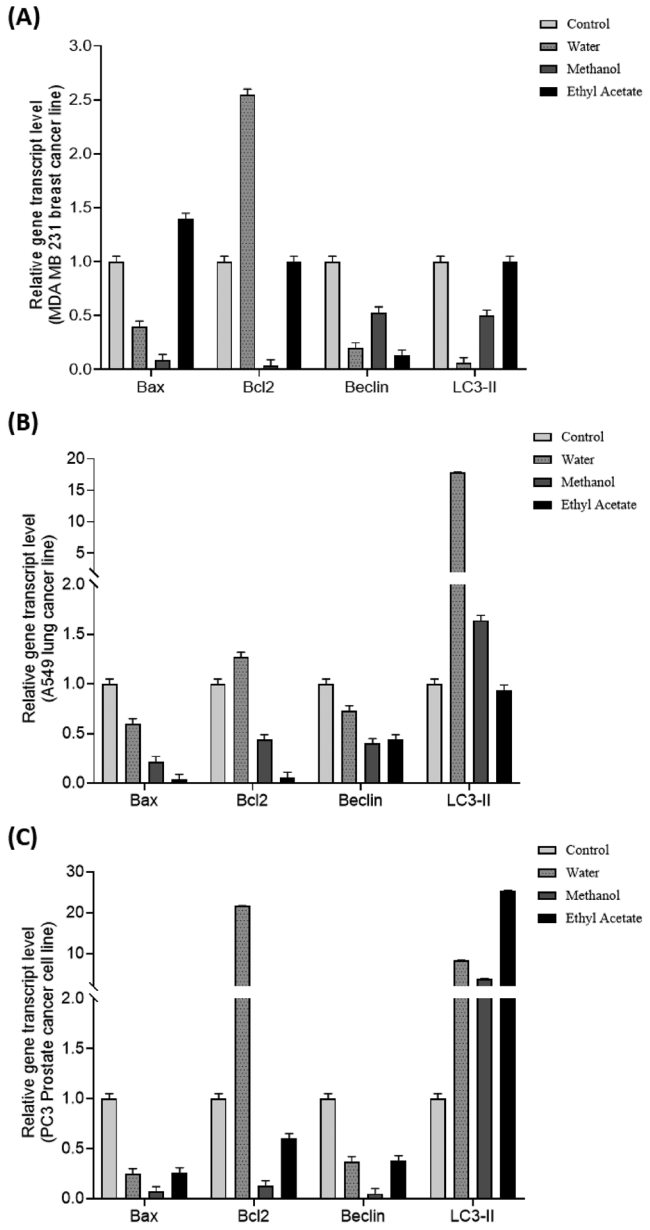


FIGURE 4 | Relative gene transcript expression: (A) MDA MB 231 breast; (B) A549 lung; (C) PC3 prostate cancer lines. Values expressed are means of 3 measurements.

through the utilization of the STRING database for the analysis of data pertaining to breast cancer (Figure 6A). The maximal clique centrality (MCC) technique, as implemented via the CytoHubba plugin, revealed the presence of multiple important hub genes, including TP53, STAT3, CTNNB1, and HIF1A (Figure 6B).

The STRING analysis of prostate cancer, comprising 37 edges and 387 nodes, yielded a more comprehensive network (Figure 7A). A notable finding was the identification of TP53, PTEN, CDKN2A, and PIK3CA as key hub genes (Figure 7B).

A network comprising 591 nodes and 10,632 edges was generated by the STRING database analysis in the context of lung cancer (Figure 8A). The hub genes were identified by the MCC approach as TP53, MYC, ACTB, and BCL2 (Figure 8B).

3.8 | KEGG Analysis of Cancer-related Molecular Pathways of *L. orientalis* Compounds

A target pathway enrichment study was performed using the DAVID 6.8 tool to investigate the possible biological effects of *L. orientalis* components on breast, prostate, and lung cancer. The study identified 102 pathways associated with prostate cancer, 161 pathways associated with lung cancer, and 145 pathways associated with breast cancer based on statistical significance ($p < 0.05$). It was found that *L. orientalis* components enhanced a number of significant biological processes associated with cancer (Figure 9). This level of enrichment reflects the proportional relevance of each pathway. The pathways highlighted in red are statistically more significant and have lower p values, whereas the pathways highlighted in blue suggest pathways of lower significance. In addition, the number of targeted molecules involved in each pathway is indicated by the size of the circles in the figure; larger circles indicate a higher number of molecules associated with that particular biological pathway. These findings provide important new insights into the potential pharmaceutical uses of *L. orientalis*. Among the biological pathways shown in the plot (Figure 9), pathways including the MAPK signaling system, microRNAs in cancer, and the PI3K–Akt signaling pathway are significant. The enrichment of these pathways suggests that the chemicals present in *L. orientalis* may be relevant to the biology of both cancer and cardiovascular disease. An important mechanism associated with angiogenesis, proliferation, and cell survival is the PI3K–Akt pathway, suggesting that *L. orientalis* may have an impact on these biological processes. The enrichment of the lipid and atherosclerosis pathway suggests that the plant may have an effect on diseases associated with atherosclerosis and cholesterol accumulation.

The analysis of cancer-related pathways also shows that the molecules from *L. orientalis* show a significant enrichment in the biological pathway "MicroRNAs in cancer." This suggests that certain biochemical pathways involved in the development of cancer could be targeted by the plant's compounds. This is particularly true for cancers, such as breast, prostate, and lung, suggesting that the plant may disrupt the cellular processes that give rise to these tumors. In particular, prostate cancer enrichment of pathways, including PI3K–Akt and MAPK signaling, was substantial. Prostate cancer progression is largely dependent on the PI3K–Akt pathway, which is essential for cell proliferation and survival. Breast cancer: There was a significant enrichment of microRNAs and proteoglycans in the cancer pathways. Although microRNAs control gene expression and play a role in breast cancer development, proteoglycans are involved in altering the tumor microenvironment. Lung cancer: Pathways, such as chemical carcinogenesis—reactive oxygen species and cellular senescence, were significantly enriched. Reactive oxygen species are known to drive mutations that lead to lung cancer, and cellular senescence plays a role in its progression.

It is well known that signals that support the growth and survival of cancer cells depend on the MAPK pathway. *L. orientalis* may stop the growth and spread of cancer cells by specifically targeting this pathway. MicroRNAs are an important additional mechanism in the control of immunological responses and inflammation. The enrichment of this pathway suggests that *L. orientalis* may have anti-inflammatory properties and may be

26438429, 2025, 3, Downloaded from https://iadns.onlinelibrary.wiley.com/doi/10.1002/ffd2.545 by Turkey Cochrane Evidence Aid, Wiley Online Library on [26/10/2026]. See the Terms and Conditions (https://onlinelibrary.wiley.com/terms-and-conditions) on Wiley Online Library for rules of use; OA articles are governed by the applicable Creative Commons License

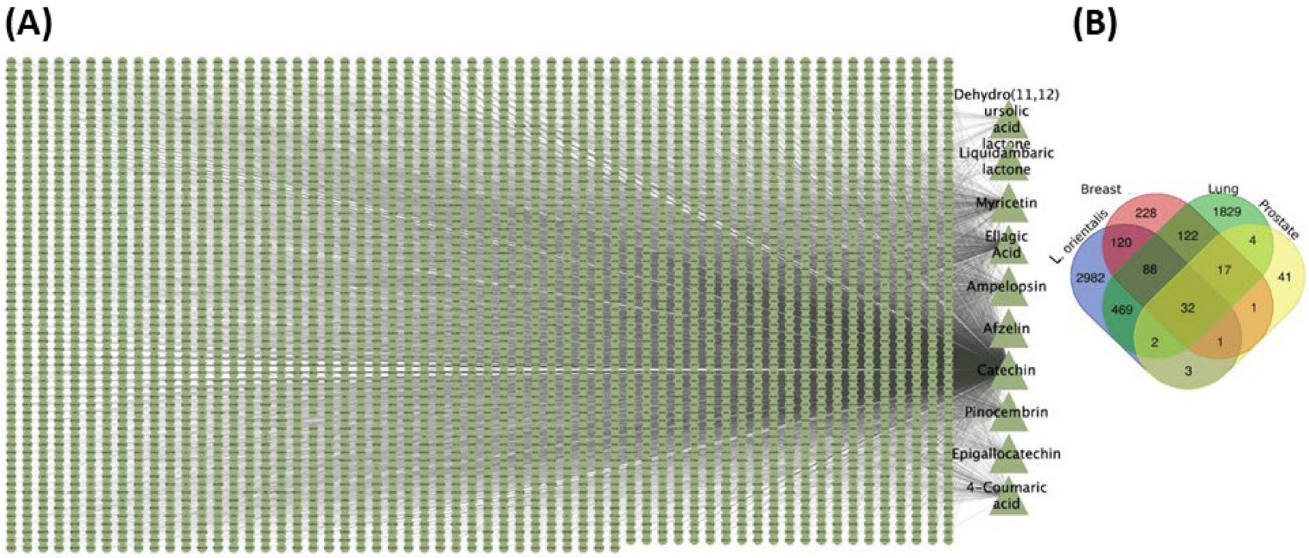


FIGURE 5 | Target analysis of *Liquidambar orientalis* and cancer: (A) target analysis of *L. orientalis*; (B) Venn diagram showing the overlap between *L. orientalis*–related breast, lung, and prostate cancer-associated genes.

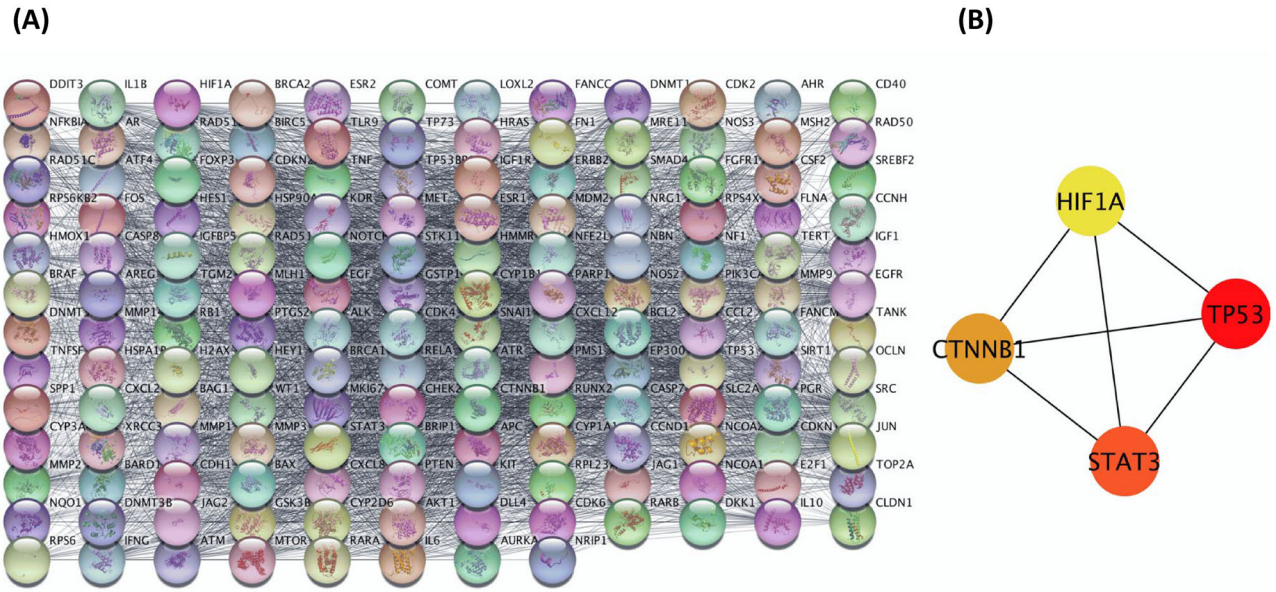


FIGURE 6 | Target analysis of *Liquidambar orientalis* and breast cancer. (A) 152 nodes and 3981 edges, and (B) TP53, STAT3, CTNNB1, and HIF1A, as multiple important hub genes, were identified in a gene interaction network.

useful in the treatment of inflammation-driven malignancies. These results suggest a potential role for the plant in immunological modulation. Taken together, these findings demonstrate the medicinal potential of *L. orientalis* components in the treatment of serious diseases such as cancer and heart disease. The enrichment of pathways related to cancer biology (PI3K–Akt, MAPK signaling, and microRNAs) suggests that *L. orientalis* may be a valuable pharmacological resource and may offer new targets for the treatment of cancer. Furthermore, the plant shows improved molecular pathways related to lipid metabolism and atherosclerosis, suggesting potential benefits against cardiovascular disease. Therefore, the results of our KEGG enrichment analysis suggest the potential of *L. orientalis* as a therapeutic agent for serious diseases such as cancer and cardiovascular diseases.

3.9 | External Verification of Primary Objectives: mRNA Expression Levels of Essential Targets

This study finds common gene targets between prostate, lung, and breast malignancies and phytochemicals derived from *L. orientalis*. After identifying the common targets, important core genes were found using the CytoHubba plugin. In the first part, the expression levels of the genes ACTB, BCL2, CDKN2A,

26438429, 2025, 3, Downloaded from https://adsn.onlinelibrary.wiley.com/doi/10.1002/ff2.545 by Turkey Cochrane Evidence Aid, Wiley Online Library on [26/10/2026]. See the Terms and Conditions (https://onlinelibrary.wiley.com/terms-and-conditions) on Wiley Online Library for rules of use; OA articles are governed by the applicable Creative Commons License

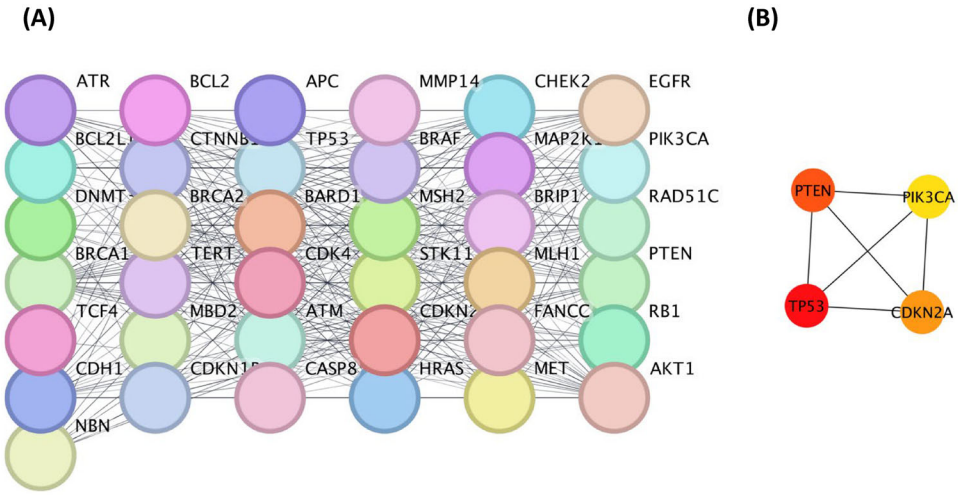


FIGURE 7 | Target analysis of *Liquidambar orientalis* and prostate cancer.(A) 387 nodes and 37 edges, and (B) TP53, PTEN, CDKN2A, and PIK3CA, as multiple important hub genes, were identified in a gene interaction network.

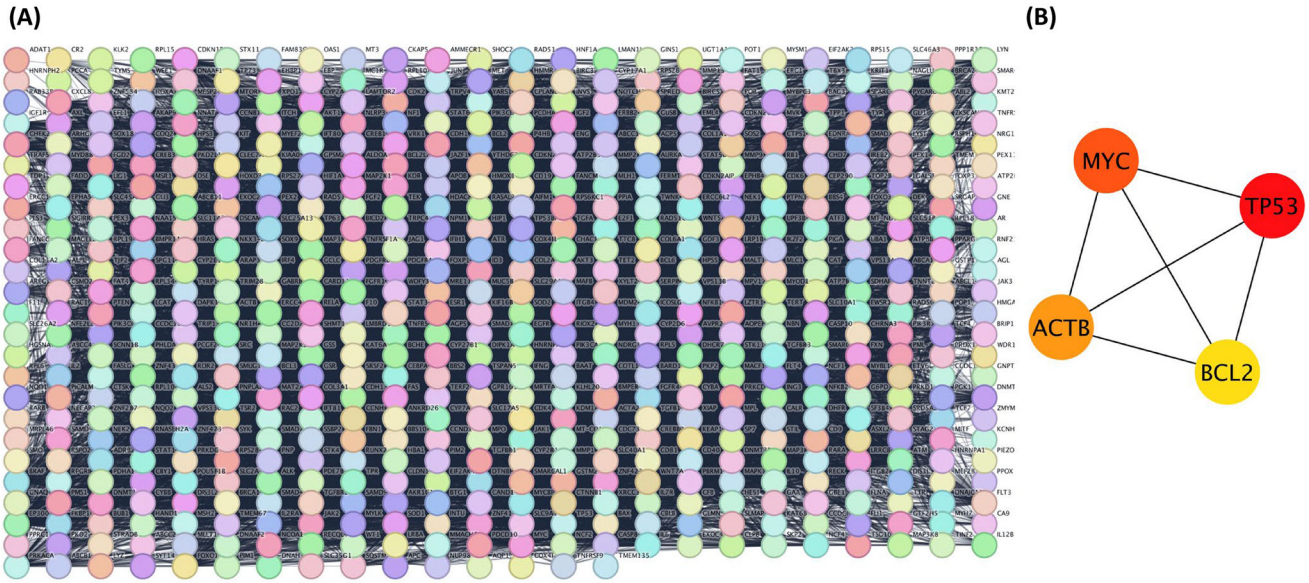


FIGURE 8 | Target analysis of *Liquidambar orientalis* and lung cancer.(A) 591 nodes and 10,632 edges, and (B) TP53, MYC, ACTB, and BCL2, as multiple important hub genes, were identified in a gene interaction network.

CTNNB1, HIF1A, MYC, PIK3CA, PTEN, STAT3, and TP53 in breast, lung, and prostate cancer were examined. The results showed significant overexpression of BCL2 and CDKN2A in cancer tissues, suggesting that these genes may be important for cancer initiation and progression. Significant alterations were also found in other genes, including TP53, HIF1A, and CTNNB1.

These results provide valuable information for the identification of putative therapeutic targets in cancer biology. The expression levels of the selected genes are examined in Figure 10B in relation to the different stages of lung and breast cancer. Because STAT3 expression is particularly high in Stage II breast cancer, it is possible that this gene is essential for disease progression. Similarly, the expression levels of TP53 and STAT3 varied among stages. BCL2 was significantly hypoexpressed in Stage IV lung cancer, suggesting that this gene may have different biological functions in later stages of the disease. Conversely, TP53 showed relatively constant expression levels in lung and breast tumors, with a slight decrease in more advanced stages. Collectively, these results indicate the need to further investigate the role of genes such as BCL2, CDKN2A, STAT3, and TP53 in cancer biology, either as biomarkers or as therapeutic targets in disease progression. Variations in the expression levels of these genes may be important for understanding the underlying causes of cancer and developing therapeutic approaches. Identifying the core genes by the CytoHubba plugin has contributed to our understanding of the links between *L. orientalis* and different types of cancer. It has highlighted the importance of these genes as potential targets for treatment.

26438429, 2025, 3, Downloaded from https://iadns.onlinelibrary.wiley.com/doi/10.1002/ffd2.545 by Turkey Cochrane Evidence Aid, Wiley Online Library on [26/10/2026]. See the Terms and Conditions (https://onlinelibrary.wiley.com/terms-and-conditions) on Wiley Online Library for rules of use; OA articles are governed by the applicable Creative Commons License

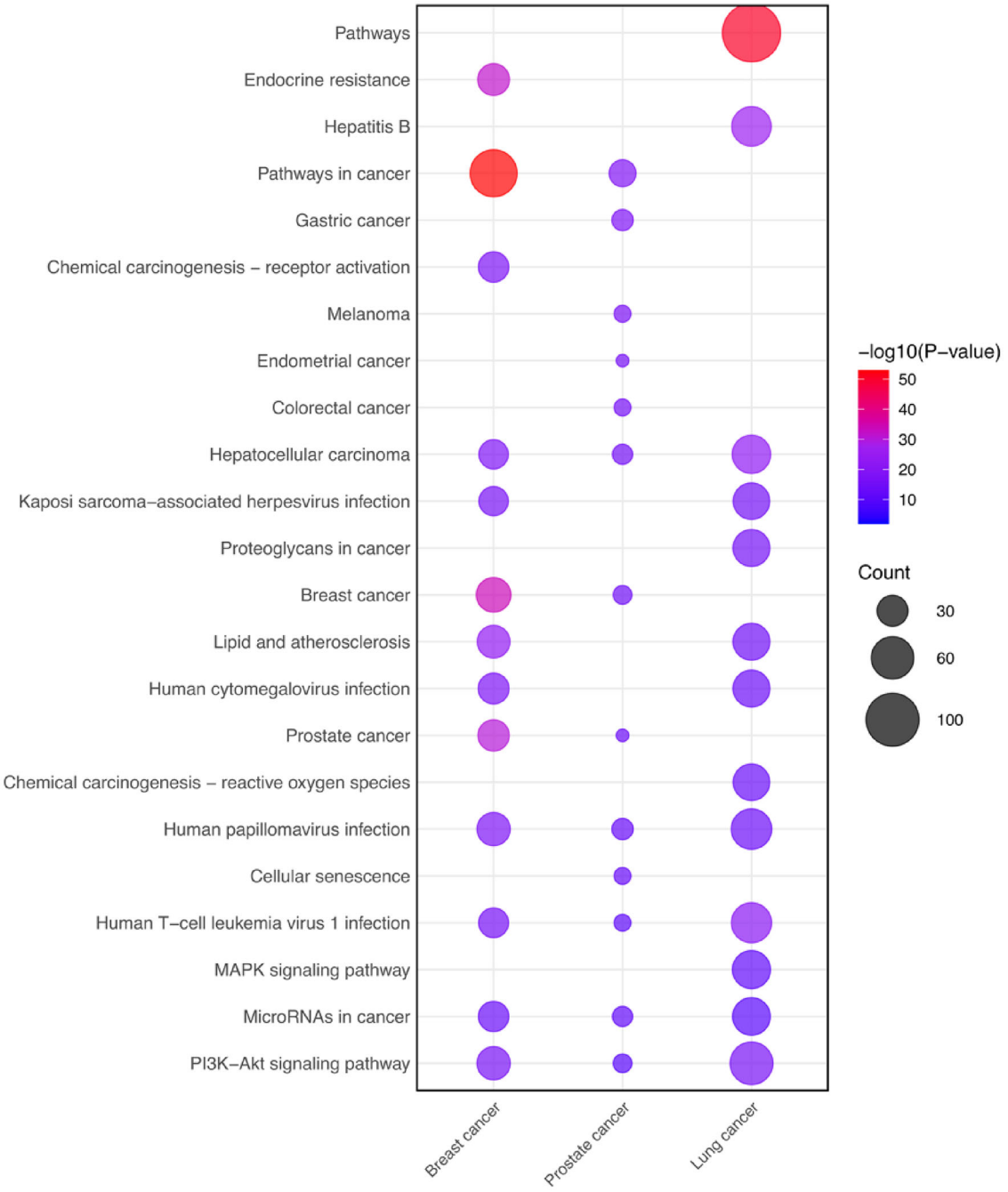


FIGURE 9 | Cancer-related term enrichment analysis using KEGG pathways shows the KEGG pathway enrichment analysis for the 13 most related pathways to cancer types.

3.10 | Evaluating Docking Outcomes: Ligand-Binding Energies and Interaction Profiles

This study used a comprehensive evaluation approach to investigate the properties of compounds identified in *L. orientalis* against specific bacterial enzymes, cancer-related proteins, and standard enzymes (Figure 11). The coordinates and grid sizes used in the analyses are shown in Table S1. Chemical profiling revealed a significant number of bioactive compounds, including liquidambaric lactone, catechin, afzelin, myricetin, epigallocatechin, and ampelopsin. The standard enzymes AChE, BChE, Tyr, amylase, and glucosidase were analyzed along with key proteins from *S. aureus* and *E. coli* and targets from breast, lung, and prostate cancers. These targets included 30S ribosomal protein S3, dihydropteroate synthase, gyrase B, MurE, transpeptidase, aromatase, BCL-2, EGFR, TP53, CASP-3, HDAC6, PDK3, AR, ESR1, HSP90AA1, PPARG, PTGS2, and CDKN2A. The primary objective was to explore the antimicrobial and anticancer activities of these phytochemicals in relation to both bacterial and cancer-related proteins, as well as standard enzymes. Table 7 highlights compounds with binding energies below −9 kcal/mol, whereas Table S2 lists those with binding energies above this threshold. The docking results showed a range of binding energies from −13.3 to −3.1 kcal/mol (Table S2).

26438429, 2025, 3, Downloaded from https://iadns.onlinelibrary.wiley.com/doi/10.1002/ffd2.545 by Turkey Cochrane Evidence Aid, Wiley Online Library on [26/10/2026]. See the Terms and Conditions (https://onlinelibrary.wiley.com/terms-and-conditions) on Wiley Online Library for rules of use; OA articles are governed by the applicable Creative Commons License

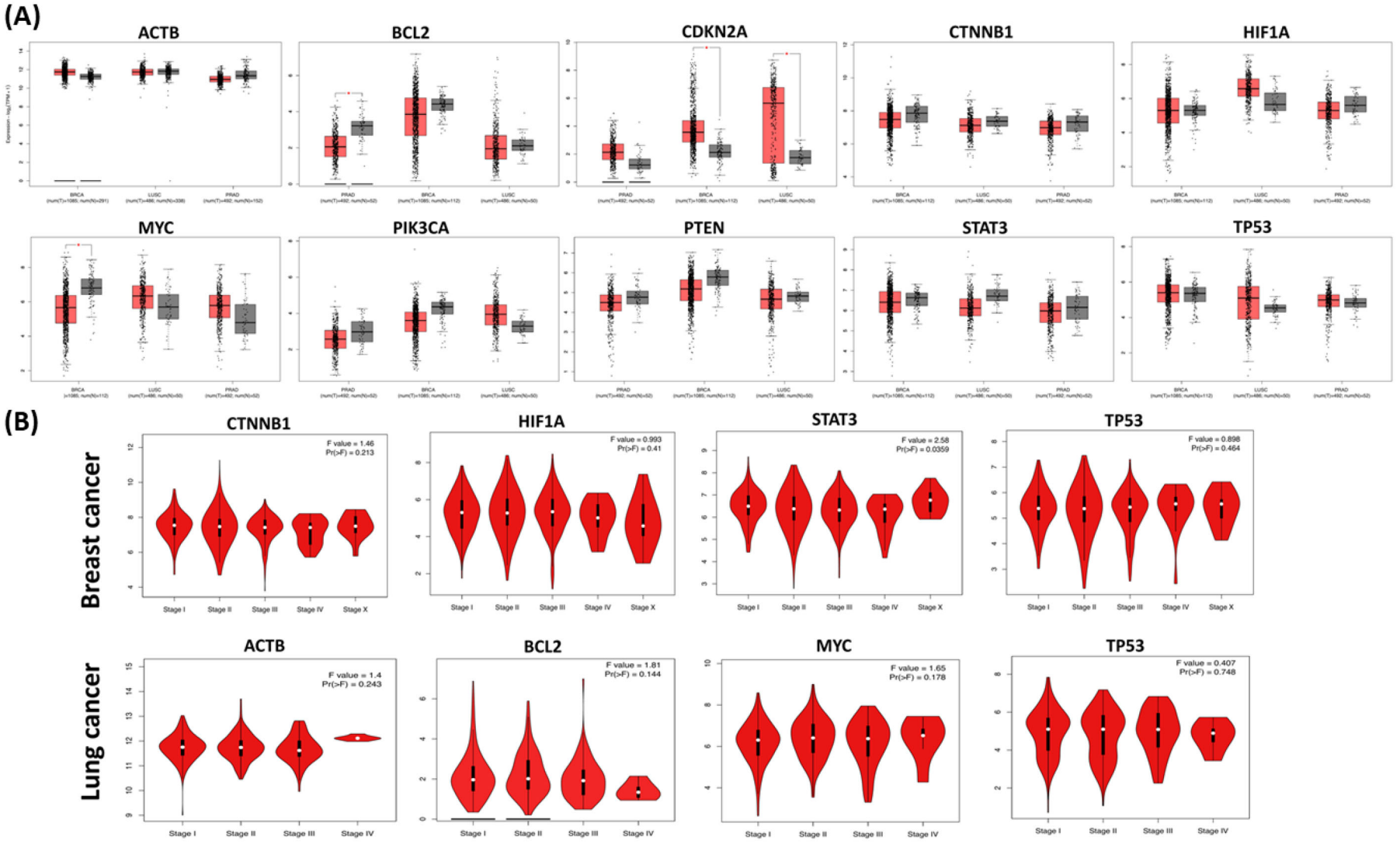


FIGURE 10 | mRNA expression levels of essential targets in various cancer types.

26438429, 2025, 3, Downloaded from https://iadns.onlinelibrary.wiley.com/doi/10.1002/ffd2.545 by Turkey Cochrane Evidence Aid, Wiley Online Library on [26/10/2026]. See the Terms and Conditions (https://onlinelibrary.wiley.com/terms-and-conditions) on Wiley Online Library for rules of use; OA articles are governed by the applicable Creative Commons License

TABLE 7 | The docking score (kcal/mol) and interacting residues of the enzyme and protein.

Compound	Target	PDB ID	Binding energy	RMSD	Interaction		Binding site
					Type	Number	
Liquidambaric lactone	*PTGS2*	5F19	−9.6	0.01	H-bond	5	SER A:126; GLN A:372; LYS A:532; ARG A:61
Catechin	*PTGS2*	5F19	−9.0	0.72	H-bond	5	ASN A:34; CYS A:47; CYS A:47; GLN A:461; GLN A:461
Afzelin	*PTGS2*	5F19	−9.0	0.94	H-bond	8	PHE A:210; PHE A:210; THR A:212; HIS A:388; HIS A:207; HIS A:386; HIS A:388
Myricetin	*PTGS2*	5F19	−9.1	5.81	H-bond	5	ASN A:34; GLY A:45; CYS A:47; GLN A:461; GLN A:461
Epigallocatechin	*PTGS2*	5F19	−9.0	8.50	H-bond	7	ASN A:34; ASN A:34; CYS A:47; CYS A:47; TYR A:130; GLN A:461; GLN A:461
Ampelopsin	*PTGS2*	5F19	−9.1	8.92	H-bond	6	CYS A:36; ARG A:44; ARG A:44; ARG A:44; ARG A:469; ARG A:469
Catechin	*HSP90AA1*	5FWK	−9.1	0.79	H-bond	8	LYS A:53; GLY A:109; THR A:110; PHE A:129; GLY A:130; VAL A:131; GLY A:132; PHE A:133
Afzelin	*HSP90AA1*	5FWK	−9.1	1.06	H-bond	8	ASN A:46; LYS A:53; GLY A:127; PHE A:129; GLY A:130; PHE A:133; LYS A:53
Myricetin	*HSP90AA1*	5FWK	−9.5	0.90	H-bond	10	LYS A:53; ASP A:88; GLY A:109; THR A:110; PHE A:129; GLY A:130; VAL A:131; VAL A:131; GLY A:132; PHE A:133
Epigallocatechin	*HSP90AA1*	5FWK	−9.2	0.73	H-bond	9	LYS A:53; ASP A:88; GLY A:109; THR A:110; PHE A:129; GLY A:130; VAL A:131; GLY A:132; PHE A:133
Ampelopsin	*HSP90AA1*	5FWK	−9.5	0.98	H-bond	9	LYS A:53; GLY A:109; THR A:110; PHE A:129; GLY A:130; VAL A:131; VAL A:131; GLY A:132; PHE A:133

(Continues)

26438429, 2025, 3, Downloaded from https://iadns.onlinelibrary.wiley.com/doi/10.1002/ffd.5545 by Turkey Cochrane Evidence Aid, Wiley Online Library on [26/10/2026]. See the Terms and Conditions (https://onlinelibrary.wiley.com/terms-and-conditions) on Wiley Online Library for rules of use; OA articles are governed by the applicable Creative Commons License

TABLE 7 | (Continued)

Compound	Target	PDB ID	Binding energy	RMSD	Interaction		Binding site
					Type	Number	
Liquidambaric lactone	*HDAC6*	5EDU	−13.3	0.00	H-bond	0	
Afzelin	*HDAC6*	5EDU	−9.1	0.72	H-bond	7	LYS B:123; TRP B:170; ALA B:171; ASP B:173; ARG B:174; ARG B:174; ASN B:258
Ellagic acid	*HDAC6*	5EDU	−9.5	7.25	H-bond	7	ASN B:120; LYS B:123; GLU B:152; GLU B:152; ARG B:174; GLU B:219; GLU B:261
Pinocembrin 5-7-Dihydroxyflavanone	*HDAC6*	5EDU	−9.2	0.91	H-bond	1	GLU B:219
Liquidambaric lactone	*PPARG*	1FM6	−9.4	0.00	H-bond	1	GLN D:345
Liquidambaric lactone	*EGFR*	1m17	−10.2	0.03	H-bond	10	ALA A:719; LYS A:721; LYS A:721; GLU A:738; THR A:766; ARG A:817; ASN A:818; THR A:830; ASP A:831; ASP A:831
Afzelin	*EGFR*	1m17	−9.6	1.03	H-bond	10	ALA A:719; LYS A:721; LYS A:721; GLU A:738; THR A:766; ARG A:817; ASN A:818; THR A:830; ASP A:831; ASP A:831
Liquidambaric lactone	*Aromatase*	4gl7	−9.4	0.01	H-bond	2	GLN A:351; LYS A:448
Afzelin	*Aromatase*	4gl7	−9.3	0.08	H-bond	5	ARG A:115; ARG A:115; TRP A:141; THR A:310; ARG A:435
Liquidambaric lactone	*TP53*	6mxy	−9.6	0.00	H-bond	1	ASP A:1521
Liquidambaric lactone	*Casp-3*	3gjq	−9.6	0.09	H-bond	1	THR C:62
Liquidambaric lactone	*BCL-2*	6O0K	−9.1	0.10	H-bond	0	
Liquidambaric lactone	*BChE*	3djy	−11.7	0.18	H-bond	1	ASP A:70
Catechin	*BChE*	3djy	−9.2	0.78	H-bond	4	ASP A:70; ASP A:70; GLU A:197; TYR A:332
Afzelin	*BChE*	3djy	−10.2	0.42	H-bond	9	TRP A:82; GLY A:115; GLY A:116; GLY A:117; TYR A:128; TYR A:128; ALA A:199; TYR A:332; HIS A:438
Myricetin	*BChE*	3djy	−9.3	0.34	H-bond	8	ASP A:70; ASP A:70; ASN A:83; ASN A:83; GLU A:197; TYR A:332; TYR A:332; HIS A:438

(Continues)

26438429, 2025, 3, Downloaded from https://iadns.onlinelibrary.wiley.com/doi/10.1002/fft2.545 by Turkey Cochrane Evidence Aid, Wiley Online Library on [26/10/2026]. See the Terms and Conditions (https://onlinelibrary.wiley.com/terms-and-conditions) on Wiley Online Library for rules of use; OA articles are governed by the applicable Creative Commons License

TABLE 7 | (Continued)

Compound	Target	PDB ID	Binding energy	RMSD	Interaction		Binding site
					Type	Number	
Ellagic acid	*BChE*	3djy	−9.1	0.10	H-bond	7	ASP A:70; ASP A:70; ASP A:70; GLY A:115; TYR A:332; HIS A:438
Epigallocatechin	*BChE*	3djy	−9.7	0.23	H-bond	3	ASN A:68; ASP A:70; TYR A:332
Ampelopsin	*BChE*	3djy	−9.4	0.06	H-bond	5	ASP A:70; ASP A:70; ASP A:70; GLU A:197; TYR A:332
Liquidambaric lactone	*Amylase*	2qv4	−11.0	0.00	H-bond	0	0
Afzelin	*Amylase*	2qv4	−9.3	0.71	H-bond	8	ARG A:195; ARG A:195; ASP A:197; LYS A:200; HIS A:201; GLU A:233; HIS A:299; HIS A:305
Myricetin	*Amylase*	2qv4	−9.3	0.74	H-bond	4	GLN A:63; ARG A:195; ASP A:197; HIS A:299
Epigallocatechin	*Amylase*	2qv4	−9.0	0.11	H-bond	4	TYR A:62; GLN A:63; ASP A:197; HIS A:299
Liquidambaric lactone	*Glucosidase*	3w37	−9.2	0.00	H-bond	3	ASN A:668; ARG A:536
Liquidambaric lactone	*AChE*	2y2v	−10.2	0.00	H-bond	1	TYR A:72
Catechin	*AChE*	2y2v	−9.6	1.02	H-bond	5	TYR A:72; ASP A:74; ASN A:87; GLY A:120; TYR A:133
Afzelin	*AChE*	2y2v	−11.0	0.98	H-bond	7	GLN A:71; ASP A:74; ASN A:87; TYR A:124; ALA A:204; TYR A:341; HIS A:447
Epigallocatechin	*AChE*	2y2v	−9.8	0.21	H-bond	6	GLN A:71; TYR A:72; ASP A:74; ASP A:74; GLY A:120; TYR A:133
Ellagic acid	*AChE*	2y2v	−9.6	0.48	H-bond	8	ASP A:74; ASN A:87; ASN A:87; GLY A:126; TYR A:133; TYR A:337; TYR A:341; HIS A:447
Ampelopsin	*AChE*	2y2v	−9.4	1.06	H-bond	3	ASP A:74; ASN A:87; GLY A:120

(Continues)

26438429, 2025, 3, Downloaded from https://iadns.onlinelibrary.wiley.com/doi/10.1002/ffd2.545 by Turkey Cochrane Evidence Aid, Wiley Online Library on [26/10/2026]. See the Terms and Conditions (https://onlinelibrary.wiley.com/terms-and-conditions) on Wiley Online Library for rules of use; OA articles are governed by the applicable Creative Commons License

TABLE 7 | (Continued)

Compound	Target	PDB ID	Binding energy	RMSD	Interaction		Binding site
					Type	Number	
Pinocembrin 5-7-dihydroxyflavanone	*AChE*	2y2v	−9.7	0.80	H-bond	2	GLY A:121; GLY A:122
Liquidambaric lactone	*S. aureus Gyrase B*	4URN	−9.2	0.01	H-bond	1	TYR A:72
Liquidambaric lactone	*E. coli MurE*	1E8C	−9.2	0.04	H-bond	1	ARG B:29
Afzelin	*E. coli MurE*	1E8C	−9.4	0.44	H-bond	11	THR B:120; THR B:120; ASP B:209; HIS B:210; HIS B:359; GLY B:386; ARG B:389; LYS B:393; HIS B:210; HIS B:359
Pinocembrin 5-7-dihydroxyflavanone	*S. aureus MurE*	4C13	−9.8	0.57	H-bond	7	GLY A:113; LYS A:114; THR A:115; THR A:115; THR A:115; SER A:116; ARG A:335
Myricetin	*S. aureus MurE*	4C13	MurE 9.8	4.76	H-bond	11	GLY A:113; LYS A:114; THR A:115; THR A:115; SER A:116; THR A:137; GLU A:177; HIS A:205; ARG A:335; HIS A:353; GLY A:357
Liquidambaric lactone	*S. aureus MurE*	4C13	−9.4	0.00	H-bond	1	SER A:42
Epigallocatechin	*S. aureus MurE*	4C13	−10.0	0.44	H-bond	11	THR A:111; GLY A:113; LYS A:114; THR A:115; THR A:115; SER A:116; SER A:116; ASN A:301; ARG A:335; ARG A:335; GLY A:357
Ellagic acid	*S. aureus MurE*	4C13	−9.1	0.28	H-bond	13	THR A:111; GLY A:113; LYS A:114; LYS A:114; THR A:115; THR A:115; SER A:116; ASP A:350; HIS A:353; THR A:354; ARG A:335; HIS A:353
Catechin	*S. aureus MurE*	4C13	−9.9	0.94	H-bond	10	GLY A:113; LYS A:114; SER A:116; ASN A:301; ASN A:301; ARG A:335; ASP A:350; TYR A:351; HIS A:353; HIS A:353
Ampelopsin	*S. aureus MurE*	4C13	−9.7	0.33	H-bond	12	THR A:111; GLY A:113; LYS A:114; THR A:115; THR A:115; SER A:116; SER A:116; ASN A:301; ARG A:335; ARG A:335; GLY A:357

(Continues)

26438429, 2025, 3, Downloaded from https://iadns.onlinelibrary.wiley.com/doi/10.1002/ffd2.545 by Turkey Cochrane Evidence Aid, Wiley Online Library on [26/10/2026]. See the Terms and Conditions (https://onlinelibrary.wiley.com/terms-and-conditions) on Wiley Online Library for rules of use; OA articles are governed by the applicable Creative Commons License

TABLE 7 | (Continued)

Compound	Target	PDB ID	Binding energy	RMSD	Interaction		Binding site
					Type	Number	
Afzelin	*S. aureus MurE*	4C13	−9.6	0.82	H-bond	16	LYS A:114; LYS A:114; THR A:115; THR A:115; ASN A:151; GLU A:177; HIS A:205; HIS A:353; ARG A:383; ARG A:383; ASN A:407; HIS A:205; HIS A:353; LYS A:114
Liquidambaric lactone	*S. aureus 30S ribosome S3*	5TCU	−9.3	0.00	H-bond	2	GLU B:19; ALA B:20
Afzelin	*S. aureus Transpeptidase*	5TW8	−9.1	0.42	H-bond	12	SER A:75; LYS A:78; SER A:116; SER A:116; SER A:139; SER A:139; ASN A:141; THR A:180; ALA A:182; THR A:260; SER A:262; GLU A:297
Liquidambaric lactone	*E. coli Transpeptidase*	6NTW	−9.8	0.00	H-bond	1	GLN A:216

Abbreviations: PDB, Protein Data Bank; RMSD, root mean square deviation.

The interactions highlighted in the evaluation based on RMSD, number of hydrogen bonds, and docking scores were investigated. First, liquidambaric lactone was identified as the compound with the strongest interaction with the PTGS2 enzyme in the docking analyses, with a binding energy of −9.6 kcal/mol and an RMSD value of 0.01. This compound was found to form five hydrogen bonds with residues SER A:126, GLN A:372, LYS A:532, and ARG A:61. Similarly, catechin, with a binding energy of −9.0 kcal/mol and an RMSD value of 0.72, formed five hydrogen bonds with residues ASN A:34, CYS A:47 (2), and GLN A:461 (2). Afzelin showed binding to PTGS2 with a binding energy of −9.0 kcal/mol and an RMSD value of 0.94, forming eight hydrogen bonds with residues PHE A:210 (2), THR A:212, HIS A:388 (3), HIS A:207, and HIS A:386. Furthermore, myricetin and epigallocatechin also showed strong interactions with PTGS2, forming five and seven hydrogen bonds, respectively, with binding energies of −9.1 and −9.0 kcal/mol. However, the RMSD values of these two compounds ranged from 5.81 to 8.92, and therefore, these interactions were not further investigated. These results indicate that the compounds with high PTGS2 inhibition potential can effectively bind to the target protein.

In molecular docking analyses performed with the HSP90AA1 protein, myricetin was found to have the strongest interaction with a binding energy of −9.5 kcal/mol and an RMSD value of 0.90. This compound was observed to form 10 hydrogen bonds with residues LYS A:53, ASP A:88, GLY A:109, THR A:110, PHE A:129, GLY A:130, VAL A:131 (2), GLY A:132, and PHE A:133. Catechin formed eight hydrogen bonds with a binding energy of −9.1 kcal/mol and an RMSD value of 0.79, whereas afzelin showed similar interactions in the same binding regions with a binding energy of −9.1 kcal/mol. The interactions of epigallocatechin and ampelopsin with the HSP90AA1 protein also support these findings, as both compounds formed nine hydrogen bonds. These results indicate that HSP90AA1 is an important target in cancer therapy and that these compounds have high binding potential to this protein.

Liquidambaric lactone, with a binding energy of −13.3 kcal/mol and an RMSD value of 0.00, showed the strongest inhibitory potential in the analyses carried out with HDAC6, another important target protein. This molecule was found to form nine hydrogen bonds with the following residues: ARG B:174, GLU B:219, LYS B:123, GLU B:152, and GLU B:261. An effective binding energy of −9.1 kcal/mol and an RMSD value of 0.72 were achieved by afzelin at HDAC6, resulting in the formation of seven hydrogen bonds. These results highlight the inhibitory potential of afzelin and liquidmadbioc lactone in epigenetic control, given the critical role of HDAC6 in epigenetic alterations.

The docking analyses conducted with the EGFR protein revealed that liquidambaric lactone exhibited robust interactions, with a binding energy of −10.2 kcal/mol and an RMSD value of 0.03. This compound formed 10 hydrogen bonds with the following residues: ALA A:719, LYS A:721 (2), GLU A:738, THR A:766, ARG A:817, ASN A:818, THR A:830, and ASP A:831 (2). Similarly, Afzelin exhibited a high binding energy of −9.6 kcal/mol and formed 10 hydrogen bonds, indicating a robust interaction with the same protein. Given the critical role of EGFR in cell proliferation, these compounds demonstrate promise as inhibitors for cancer treatment.

26438429, 2025, 3, Downloaded from https://iadns.onlinelibrary.wiley.com/doi/10.1002/ffd2.545 by Turkey Cochrane Evidence Aid, Wiley Online Library on [26/10/2026]. See the Terms and Conditions (https://onlinelibrary.wiley.com/terms-and-conditions) on Wiley Online Library for rules of use; OA articles are governed by the applicable Creative Commons License

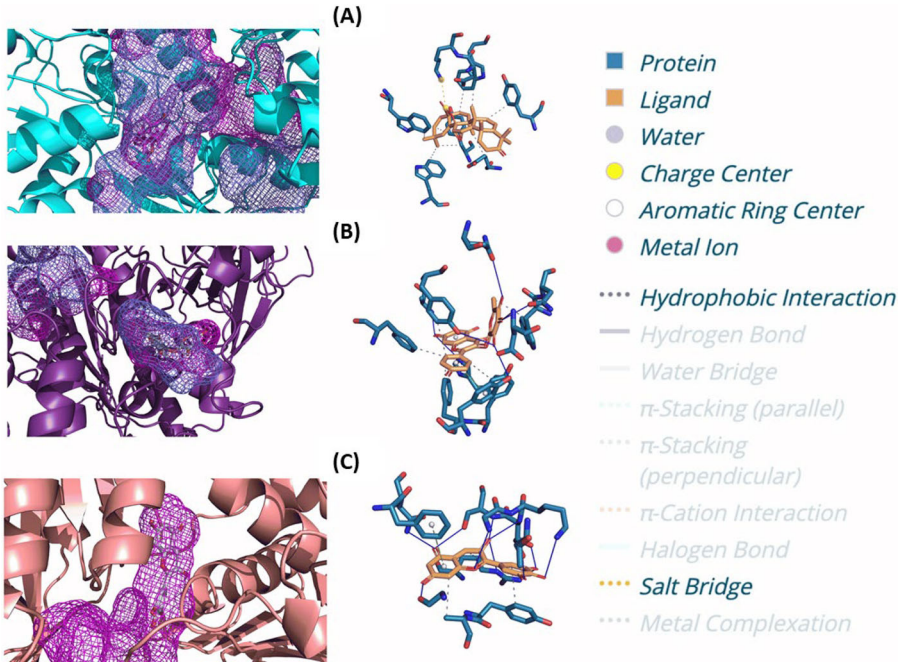


FIGURE 11 | Enzymes and proteins' active sites with compounds showing the best binding energy. (A) Interaction between PTGS2 and liquidambaric lactone—liquidambaric lactone forms key hydrophobic interactions with residues ARG44, ARG61, PHE371, and GLN372, which stabilize its binding within the active site of PTGS2. Additionally, it establishes strong hydrogen bonds with SER126, GLN372, and LYS532, enhancing its affinity. A significant salt bridge is observed with ARG61, indicating robust electrostatic interactions. These interactions suggest the compound's potential to inhibit PTGS2 activity, a key enzyme in inflammatory pathways. (B) Interaction between AChE and afzelin: Afzelin demonstrates extensive hydrophobic interactions with residues TRP86, TYR124, PHE297, TYR337, and PHE338, contributing to its stable binding within the AChE active site. Key hydrogen bonds are formed with GLN71, ASP74, ASN87, TYR124, ALA204, TYR341, and HIS447, supporting its strong affinity for the enzyme. Additionally, π-stacking interactions with residues TYR341 and HIS447 further stabilize the complex. These interactions highlight afzelin's potential role as an acetylcholinesterase inhibitor, which could be beneficial in managing neurodegenerative conditions. (C) Interaction between *S. aureus* MurE and epigallocatechin: Epigallocatechin forms strong hydrophobic interactions with residues ARG335, TYR351, and ALA352, stabilizing its position in the active site of MurE. It also establishes multiple hydrogen bonds with residues THR111, GLY113, LYS114, THR115, SER116, ASN301, and ARG335, which reinforce its binding affinity. Furthermore, π-stacking interactions with residue PHE300 enhance the complex's stability. These interactions suggest epigallocatechin's potential to disrupt peptidoglycan biosynthesis in *S. aureus*, pointing to its antibacterial properties.

Afzelin was found to have significant interactions in the docking analyses using the aromatase protein, with a binding energy of −9.3 kcal/mol and an RMSD value of 0.08. Ten hydrogen bonds were formed by this molecule with the residues ARG A:435, TRP A:141, THR A:310, and ARG A:115 (2).

Myricetin demonstrated a binding energy of −9.3 kcal/mol and an RMSD value of 0.34, forming effective hydrogen bonds with the residues GLN A:63, ARG A:195, ASP A:197, and HIS A:299 in the BChE protein analysis. Catechin demonstrated a binding energy of −9.2 kcal/mol, indicating its capacity to interact with BChE. This was evidenced by the formation of four hydrogen bonds with the residues ASP A:70 (2), GLU A:197, and TYR A:332. Afzelin exhibited robust binding to BChE, as evidenced by the formation of nine hydrogen bonds and a binding energy of −10.2 kcal/mol. Furthermore, epigallocatechin formed four hydrogen bonds with BChE, exhibiting an efficient binding energy of −9.0 kcal/mol. These findings suggest that these substances have the potential to effectively inhibit BChE activity.

In the docking analyses conducted with amylase, liquidambaric lactone was found to bind with a binding energy of −11.0 kcal/mol and an RMSD value of 0.00, forming four hydrogen bonds with the residues TYR A:62, GLN A:63, ASP A:197, and HIS A:299. Afzelin demonstrated a robust binding affinity with a binding energy of −9.3 kcal/mol and an RMSD value of 0.71, forming eight hydrogen bonds with the residues ARG A:195 (2), ASP A:197, LYS A:200, HIS A:201, GLU A:233, HIS A:299, and HIS A:305. Myricetin exhibited a binding energy of −9.3 kcal/mol and an RMSD value of 0.74, forming four hydrogen bonds with GLN A:63, ARG A:195, ASP A:197, and HIS A:299. Additionally, epigallocatechin was identified as an effective inhibitor of amylase, forming four hydrogen bonds with a binding energy of −9.0 kcal/mol.

In the docking analyses conducted with *E. coli* MurE, afzelin was found to exhibit robust interactions with a binding energy of −9.4 kcal/mol and an RMSD value of 0.44, forming 11 hydrogen bonds with the residues THR B:1. The amino acids ASP B:209, HIS B:210 (2), HIS B:359 (2), GLY B:386, ARG B:389, and LYS B:393 were identified as being present on the surface of the protein on 20 occasions. Similarly, in the docking analyses conducted with *S. aureus* MurE for various biomolecules, high binding energies and hydrogen bond numbers were observed. Pinocembrin 5-7-dihydroxyflavanone demonstrated a binding energy of −9.8 kcal/mol and an RMSD value of 0.57, forming seven hydrogen bonds with the residues GLY A:113, LYS A:114, THR A:115, SER A:116, and ARG A:335. Epigallocatechin demonstrated

26438429, 2025, 3, Downloaded from https://iadns.onlinelibrary.wiley.com/doi/10.1002/ffd2.545 by Turkey Cochrane Evidence Aid, Wiley Online Library on [26/10/2026]. See the Terms and Conditions (https://onlinelibrary.wiley.com/terms-and-conditions) on Wiley Online Library for rules of use; OA articles are governed by the applicable Creative Commons License

a binding energy of −10.0 kcal/mol and an RMSD value of 0.44, forming 11 hydrogen bonds with residues THR A:111 and GLY A: The residues involved in the interactions were GLY A:113, LYS A:114, THR A:115, SER A:116, ASN A:301, ARG A:335, and GLY A:357. Ellagic acid exhibited a binding energy of −9.1 kcal/mol and an RMSD value of 0.28, forming a total of 13 hydrogen bonds with residues THR A:111, GLY A:113, and LYS. A:114, THR A:115, SER A:116, ASP A:350, HIS A:353, THR A:354, and ARG A:335. Catechin, with a binding energy of −9.9 kcal/mol and an RMSD value of 0.94, formed 10 hydrogen bonds with residues GLY A:113, LYS A:114, SER A:116, ASN A:301, ARG A:335, ASP A:350, TYR A:351, and HIS A:353. Ampelopsin exhibited a binding energy of −9.7 kcal/mol and an RMSD value of 0.33, forming 12 hydrogen bonds with residues THR A:111, GLY A:113, LYS A:114, THR A:115, SER A:116, ASN A:301, ARG A:335, and GLY A:357. Afzelin demonstrated a binding energy of −9.6 kcal/mol and an RMSD value of 0.82, forming 16 hydrogen bonds with residues LYS A:114, THR A:115, ASN A:151, GLU A:177, HIS A:205, ARG A:383, and ASN A:407. Furthermore, the docking analyses conducted with *S. aureus* transpeptidase revealed that afzelin exhibited a binding energy of −9.1 kcal/mol and an RMSD value of 0.42. Additionally, 12 hydrogen bonds were formed between afzelin and residues SER A:75, LYS A:78, SER A:116, SER A:139, ASN A:141, THR A:180, ALA A:182, THR A:260, SER A:262, and GLU A:297 (Table 7).

In summary, the docking analyses demonstrated that the bioactive phytochemicals of *L. orientalis*, including afzelin, liquidambaric lactone, and epigallocatechin, exhibited robust hydrogen bonding interactions and binding affinities with bacterial enzymes, cancer-related proteins, and standard enzymes. These compounds have the potential to be employed as antibacterial and anticancer treatments, given their high binding energies and extensive hydrogen bonding. These compounds have been demonstrated to be particularly efficacious against key enzymes such as EGFR, transpeptidase, and MurE. To confirm their effectiveness and therapeutic potential, further in vivo research and experimental confirmation are required.

3.11 | Binding-Free Energy Analysis: MM/PBSA Results and Implications for Ligand Efficacy

In this study, the effect of energy components on binding stability was evaluated by calculating and analyzing a series of protein–ligand complexes. The investigation focused on several important energy parameters, including van der Waals interaction (VDWAALS), electrostatic energy (EEL), polar solvation energy (EGB), surface tension (ESURF), gas phase energy (GGAS), solvation energy (GSOLV), and total energy (TOTAL). The evaluation of cancer-related enzyme activities of phenolic derivatives derived from *L. orientalis* was performed using MM/PBSA binding free energy calculations in conjunction with MD simulations. Seven complexes were selected for further analysis based on factors such as low RMSD, high binding energy, and the number of hydrogen bonds formed. The complexes selected for further analysis are AChe_afzelin, EGFR_liquidambaric lactone, HDAC6_liquidambaric lactone, HSP90AA1_myricetin, PTGS2_liquidambaric lactone, *S. aureus* MurE_epigallocatechin, and *S. aureus*_transpeptidase afzelin, as shown in Table S3.

As shown in the figure, three complexes stand out as exhibiting exceptional binding stability. The complexes identified as having the most promising binding stability are AChe_afzelin (total energy = −43.77 kcal/mol), PTGS2_liquidambaric lactone (total energy = −28.04 kcal/mol), and *S. aureus* MurE_epigallocatechin (total energy = −30.04 kcal/mol). These complexes are highlighted in red in Table S3. In particular, the electrostatic energy value of −57.14 kcal/mol and the polar solvation energy of 65.03 kcal/mol in the AChe_afzelin complex indicate a particularly strong binding stability, as indicated by the total energy value of −43.77 kcal/mol (Figure 12). In terms of binding affinity, two other complexes are of particular interest. These are HSP90AA1_myricetin with a binding energy of −27.84 kcal/mol and *S. aureus*_transpeptidase afzelin with a binding energy of −27.24 kcal/mol. Compared to the other complexes, the EGFR_liquidambaric lactone exhibits a lower binding stability with a total energy of −21.13 kcal/mol (Table S3). Due to their low total energies and minimal fluctuations, AChe_afzelin and *S. aureus* MurE_epigallocatechin were selected for MD simulations. These complexes showed stable binding profiles with reduced energy variability, making them suitable candidates for further dynamic analysis. In conclusion, these results demonstrate that the compounds possess robust binding affinities to protein targets, suggesting their potential as inhibitor candidates and their significant contribution to drug discovery research.

3.12 | Stability and Flexibility in MD Simulation

The study aims to uncover potential therapeutic drugs through a thorough investigation of the molecular interactions between specific ligands and target proteins, with an emphasis on clarifying their binding sites. On the basis of important criteria, such as the presence of hydrogen-bonding residues, the results of MM/PBSA binding-free energy calculations, and molecular docking scores, two complexes were selected for evaluation. *S. aureus* MurE_epigallocatechin and AChe_afzelin, two ligand–protein complexes, showed robust selectivity and stability in their interactions. These complexes were subjected to MD simulations, which provided greater insight into their biological efficacy and protein binding capacities to better evaluate their potential as therapeutic agents.

Two ligand–protein complexes, AChe_afzelin and *S. aureus* MurE_epigallocatechin, were observed to remain stable throughout a 100 ns MD simulation, as evidenced by their position on the RMSD plot. The RMSD values for *S. aureus* MurE_epigallocatechin (black line) are consistently greater than those for AChe_afzelin (red line), indicating that the former exhibits comparatively higher structural stability. Throughout the simulation, the RMSD of *S. aureus* MurE_epigallocatechin exhibits a relatively stable value of approximately 0.5 nm, whereas AChe_afzelin displays a more consistent trend with an RMSD of 0.25 nm. This demonstrates that, in contrast to *S. aureus* MurE_epigallocatechin, the AChe_afzelin complex maintains its conformation with greater consistency over time. Both complexes appear to have reached equilibrium based on the comparatively stable RMSD values; however, AChe_afzelin exhibits a higher degree of stability, which may indicate a more advantageous binding configuration (Figure 13A). The flexibility of the residue level of the AChE_afzelin and *S. aureus* MurE_epigallocatechin

26438429, 2025, 3, Downloaded from https://iadns.onlinelibrary.wiley.com/doi/10.1002/ffd2.545 by Turkey Cochrane Evidence Aid, Wiley Online Library on [26/10/2026]. See the Terms and Conditions (https://onlinelibrary.wiley.com/terms-and-conditions) on Wiley Online Library for rules of use; OA articles are governed by the applicable Creative Commons License

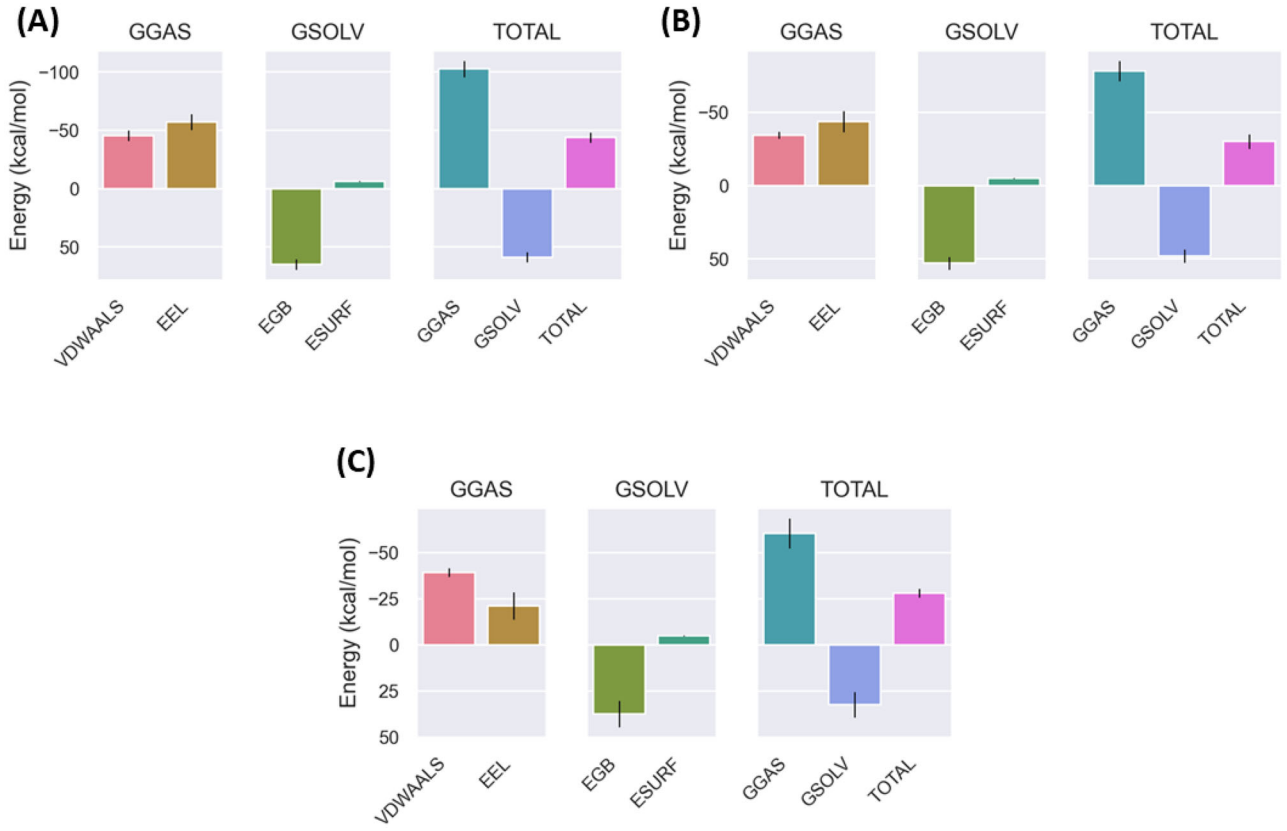


FIGURE 12 | MM/PBSA binding-free energy analysis: (A) AChe_afzelin complex; (B) PTGS2_liquidambaric lactone complex; (C) *S. aureus* MurE_epigallocatechin complex.

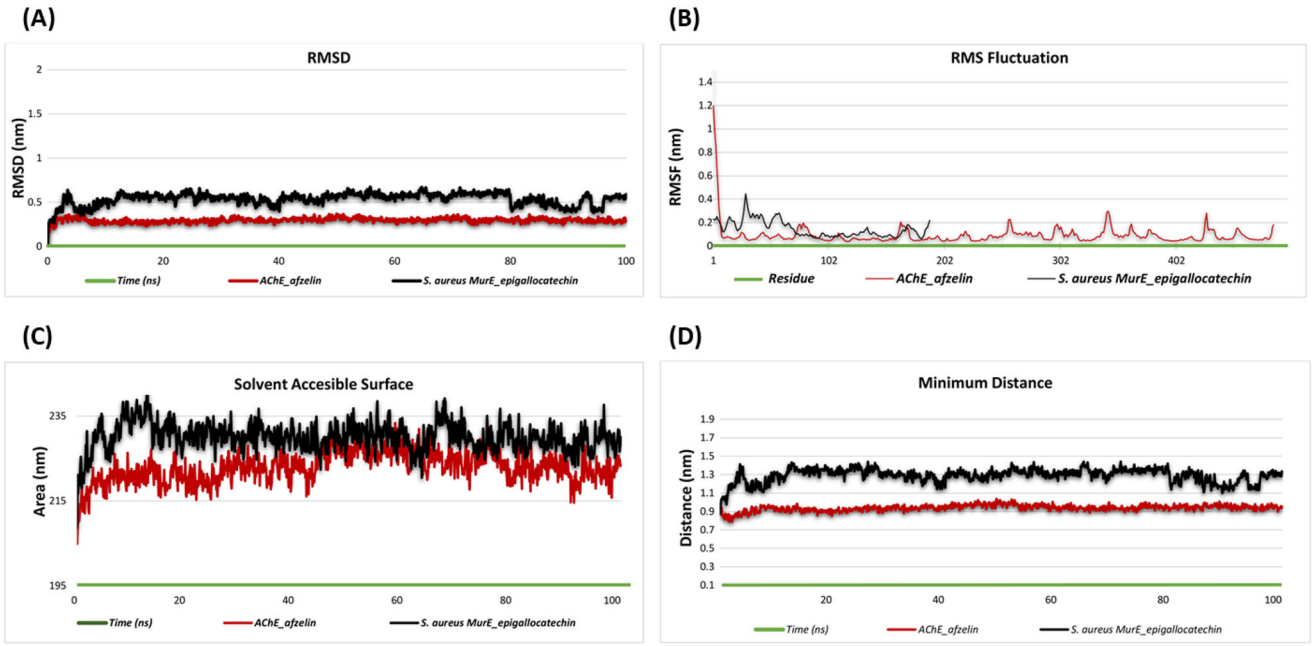


FIGURE 13 | Presentation of molecular dynamics simulations in graphical form: (A) RMSD of AChe_afzelin and *S. aureus* MurE_epigallocatechin complexes; (B) RMSF of AChe_afzelin and *S. aureus* MurE_epigallocatechin; (C) solvent accessibility of AChe_afzelin and *S. aureus* MurE_epigallocatechin complexes; (D) minimum distance of AChe_afzelin and *S. aureus* MurE_epigallocatechin complexes. RMSD, root mean square deviation.

26438429, 2025, 3, Downloaded from https://iadns.onlinelibrary.wiley.com/doi/10.1002/ffd2.545 by Turkey Cochrane Evidence Aid, Wiley Online Library on [26/10/2026]. See the Terms and Conditions (https://onlinelibrary.wiley.com/terms-and-conditions) on Wiley Online Library for rules of use; OA articles are governed by the applicable Creative Commons License

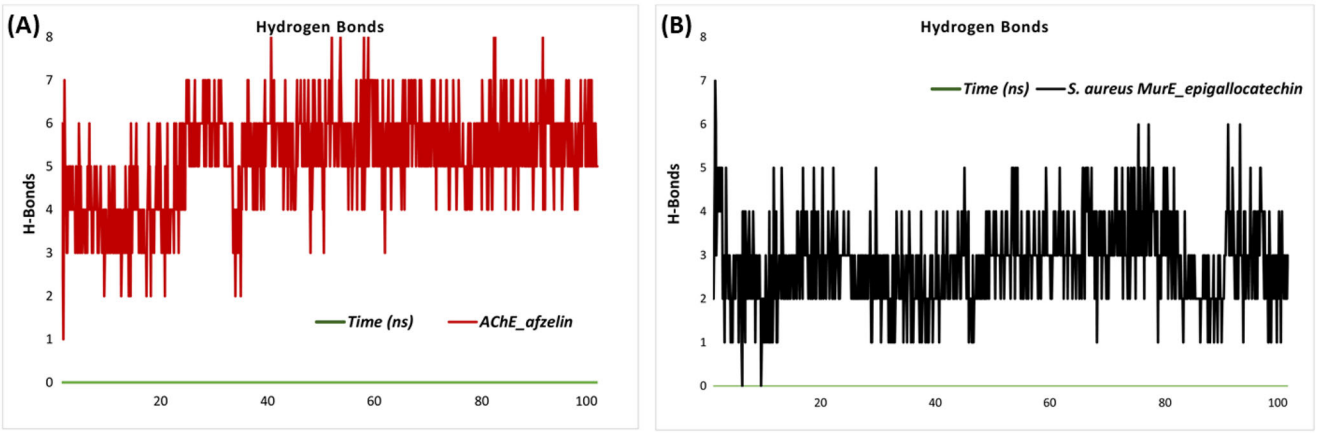


FIGURE 14 | Hydrogen bonds in complexes: (A) hydrogen bonds in AChe_afzelin complex. (B) Hydrogen bonds in *S. aureus* MurE_epigallocatechin complex.

complexes is illustrated by the root mean square fluctuation (RMSF) plot. A comparison of the AChe_afzelin and *S. aureus* MurE_epigallocatechin complexes reveals that the latter exhibits higher RMSF values, indicating greater flexibility. In the initial residues (1–30), *S. aureus* MurE_epigallocatechin displays a pronounced increase in flexibility, whereas AChe_afzelin exhibits reasonable stability in this region. Although there are slight variations in both complexes in certain areas (residues 50–70, 150–200, and 350–400), the overall pattern suggests that AChe_afzelin is less flexible over most residues. This finding suggests that the structural stability of AChe_afzelin may be attributed to its stronger conformation and capacity to maintain a stable structure at the binding site (Figure 13B). The solvent exposure of the *S. aureus* MurE_epigallocatechin and AChe_afzelin complexes is revealed by the solvent-accessible surface area (SASA) plot, which depicts the solvent exposure across a 100 ns simulation. The *S. aureus* MurE_epigallocatechin complex (black line) exhibits greater SASA values, with an average of approximately 230 nm^2, whereas the AChe_afzelin complex (red line) consistently displays lower SASA values, with an average of approximately 215 nm^2. These data suggest that *S. aureus* MurE_epigallocatechin is more solvent-exposed on its surface than AChe_afzelin, which may indicate variations in solvent interaction and conformational dynamics. Although equilibrium has been established, as indicated by the generally stable SASA values for both complexes throughout the course of the simulation, the consistently lower SASA of AChe_afzelin suggests a more compact structure, which may result in increased stability within the binding environment (Figure 13C).

The hydrogen bond (H-bond) plot for the AChE_afzelin complex illustrates the dynamic changes in H-bond numbers over a 100 ns simulation period, providing insight into the complex's hydrogen bonding dynamics. The complex maintains a range of three to eight hydrogen bonds, with fluctuations indicating transient interactions. In the initial phase of the simulation (0–20 ns), the average hydrogen bond count is relatively low, with a value of approximately three to four. However, as the simulation progresses (40–100 ns), there is an increase in the number of higher hydrogen bonds, with the average stabilizing around five to six. This trend indicates that the AChe_afzelin complex attains enhanced stability in its hydrogen bonding network over time, which likely contributes to the overall stability and specificity of the complex within the binding environment. The transient nature of the hydrogen bonds may reflect the flexibility of the binding site, which allows for conformational adjustments that improve ligand–protein affinity (Figure 14A). In contrast, the H-bond plot for the *S. aureus* MurE_epigallocatechin complex exhibits a fluctuating pattern over the same 100 ns simulation period. The complex generally maintains between one and five hydrogen bonds, with occasional peaks at seven. In the initial 20 ns, the bond count varies considerably, typically between two and four. This variability persists through the later stages (60–100 ns), with more frequent occurrences of lower counts, averaging around two to three. In comparison to the AChe_afzelin complex, this pattern indicates a less stable hydrogen bonding network, which suggests a more flexible binding environment. The fluctuations in the number of hydrogen bonds observed are likely due to conformational shifts within the binding site, which may impact the stability and ligand interaction of the complex (Figure 14B).

4 | Conclusion

Our study provided a comprehensive evaluation of the therapeutic potential of *L. orientalis* extracts, demonstrating their multifaceted biological activities, including antioxidant, antimicrobial, enzyme inhibitory, and anticancer effects. Notably, the study utilized extracts derived from the aerial parts of the plant as a whole, rather than analyzing individual parts separately. This approach allowed for the combined extraction of bioactive compounds from both leaves and stem bark, maximizing the therapeutic potential and capturing the synergistic effects of their phytochemical profiles. Our findings revealed that the methanol extract showed its superior phenolic and flavonoid content, correlating with superior antioxidant and enzyme inhibitory activities. This extract showed broad-spectrum antimicrobial efficacy and significant anticancer effects, particularly against lung cancer, by inducing autophagy. The aqueous extract demonstrated pronounced activity against prostate cancer, modulating apoptosis. In breast cancer, the ethyl acetate extract promoted apoptosis, whereas the aqueous extract enhanced autophagy.

26438429, 2025, 3, Downloaded from https://iadns.onlinelibrary.wiley.com/doi/10.1002/ffd2.545 by Turkey Cochrane Evidence Aid, Wiley Online Library on [26/10/2026]. See the Terms and Conditions (https://onlinelibrary.wiley.com/terms-and-conditions) on Wiley Online Library for rules of use; OA articles are governed by the applicable Creative Commons License

The major novelty of our study was identifying the enzyme inhibitory effects of *L. orientalis* extracts in cancer-related contexts, highlighting their dual action on apoptotic and autophagic pathways. The molecular docking and dynamic simulations further supported the therapeutic potential of key phytochemicals, such as afzelin and epigallocatechin, in targeting cancer-related enzymes and bacterial resistance mechanisms. These findings underscore the plant's value as a source of bioactive compounds for multi-targeted therapeutic applications.

By integrating traditional uses with modern pharmacological insights, this study establishes *L. orientalis* as a natural resource for developing therapies that address oxidative stress, microbial resistance, and cancer progression. Its ability to act on multiple therapeutic targets, combined with the advantages of using the aerial parts of the plant to extract a wider range of active compounds, shows it as a promising candidate for translational applications. Future research should focus on clinical validation, detailed mechanistic studies, and the influence of environmental conditions on its bioactivity to fully realize its therapeutic potential.

Conflicts of Interest

The authors declare no conflicts of interest.

References

Aboul-Soud, M. A. M., H. Ennaji, A. Kumar, et al. 2022. "Antioxidant, Anti-Proliferative Activity and Chemical Fingerprinting of *Centaurea calcitrapa* Against Breast Cancer Cells and Molecular Docking of Caspase-3." *Antioxidants* 11, no. 8: 1514. https://doi.org/10.3390/ANTIOX11081514.

Adamczak, A., M. Ożarowski, and T. M. Karpiński. 2020. "Antibacterial Activity of some Flavonoids and Organic Acids Widely Distributed in Plants." *Journal of Clinical Medicine* 9, no. 1: 109. https://doi.org/10.3390/JCM9010109.

Alkadi, H. 2020. "A Review on Free Radicals and Antioxidants." *Infectious Disorders Drug Targets* 20, no. 1: 16–26. https://doi.org/10.2174/1871526518666180628124323.

Avunduk, S., and A. Kacar. 2013. "In Vitro Biological Activity of *Liquidambar orientalis* Mill Against Pathogen and Marine Biofilm Microorganisms." *Journal of Pure and Applied Microbiology* 7, no. 4: 2885–2889.

Baloglu, M. C., L. Y. Ozer, B. Pirci, G. Zengin, A. I. Uba, and Y. C. Altunoglu. 2023. "Evaluation of the Potential Therapeutic Properties of *Liquidambar orientalis* Oil." *Chemistry & Biodiversity* 20, no. 10: e202300291. https://doi.org/10.1002/CBDV.202300291.

Bayala, B., I. H. N. Bassole, R. Scifo, et al. 2014. "Anticancer Activity of Essential Oils and Their Chemical Components—A Review." *American Journal of Cancer Research* 4, no. 6: 607.

Benvenuto, M., L. Albonici, C. Focaccetti, et al. 2020. "Polyphenol-Mediated Autophagy in Cancer: Evidence of In Vitro and In Vivo Studies." *International Journal of Molecular Sciences* 21, no. 18: 6635. https://doi.org/10.3390/IJMS21186635.

Castrejón-Jiménez, N. S., K. Leyva-Paredes, S. L. Baltierra-Uribe, et al. 2019. "Ursolic and Oleanolic Acids Induce Mitophagy in A549 Human Lung Cancer Cells." *Molecules (Basel, Switzerland)* 24, no. 19: 3444. https://doi.org/10.3390/MOLECULES24193444.

Çetinkaya, S., İ. L. Çınar Ayan, İ. P. Süntar, and H. Gül Dursun. 2022. "The Phytochemical Profile and Biological Activity of *Liquidambar orientalis* Mill. Var. Orientalis via NF-KB and Apoptotic Pathways in Human Colorectal Cancer." *Nutrition and Cancer* 74, no. 4: 1457–1473. https://doi.org/10.1080/01635581.2021.1952455.

Chang, M.-Y., and Y.-L. Shen. 2014. "Linalool Exhibits Cytotoxic Effects by Activating Antitumor Immunity." *Molecules (Basel, Switzerland)* 19, no. 5: 6694–6706. https://doi.org/10.3390/MOLECULES19056694.

Cusumano, G., G. A. Flores, M. V. Cetiz, et al. 2024. "Small Steps to the Big Picture for Health-Promoting Applications Through the Use of Chickweed (Stellaria Media): In Vitro, In Silico, and Pharmacological Network Approaches." *Food Science & Nutrition* 12, no. 11: 9295–9313. https://doi.org/10.1002/FSN3.4505.

Duangjai, A., N. Suphrom, J. Wungrath, A. Ontawong, N. Nuengchamnong, and A. Yosboonruang. 2016. "Comparison of Antioxidant, Antimicrobial Activities and Chemical Profiles of Three Coffee (*Coffea arabica* L.) Pulp Aqueous Extracts." *Integrative Medicine Research* 5, no. 4: 324–331. https://doi.org/10.1016/J.IMR.2016.09.001.

Duran, T., G. Peron, M. Zancato, et al. 2024. "Harnessing the Chemical Composition and Anti-Oxidant, Anti-Enzymatic, and Anti-Cancer Activities of Two *Corydalis* Species (*C. Erdelii* and *C. Solida*) by Using In Vitro and In Silico Analysis." *Food Bioscience* 61: 104762. https://doi.org/10.1016/J.FBIO.2024.104762.

Efe, A. 2014. "*Liquidambar orientalis* Mill. (Sığla Ağacı)'in Morfolojik Ve Palinolojik Özellikleri Üzerine Araştırmalar." *Journal of the Faculty of Forestry Istanbul University* 47, no. 2: 84–114. https://doi.org/10.17099/JFFIU.58414.

Eroğlu, C., M. Seçme, G. Bağcı, and Y. Dodurga. 2015. "Assessment of the Anticancer Mechanism of Ferulic Acid Via Cell Cycle and Apoptotic Pathways in Human Prostate Cancer Cell Lines." *Tumour Biology* 36, no. 12: 9437–9446. https://doi.org/10.1007/S13277-015-3689-3.

Ferrante, C., L. Recinella, M. Locatelli, et al. 2017. "Protective Effects Induced by Microwave-Assisted Aqueous Harpagophytum Extract on Rat Cortex Synaptosomes Challenged With Amyloid β-Peptide." *Phytotherapy Research* 31, no. 8: 1257–1264. https://doi.org/10.1002/PTR.5850.

Fiamegos, Y. C., P. L. Kastritis, V. Exarchou, et al. 2011. "Antimicrobial and Efflux Pump Inhibitory Activity of Caffeoylquinic Acids From *Artemisia absinthium* Against Gram-Positive Pathogenic Bacteria." *PLoS ONE* 6, no. 4: 1–12. https://doi.org/10.1371/JOURNAL.PONE.0018127.

Grochowski, D. M., S. Uysal, A. Aktumsek, et al. 2017. "In Vitro Enzyme Inhibitory Properties, Antioxidant Activities, and Phytochemical Profile of *Potentilla thuringiaca*." *Phytochemistry Letters* 20, no. 1: 365–372. https://doi.org/10.1016/J.PHYTOL.2017.03.005.

Gupta, A. K., Y. Vaishnav, S. K. Jain, S. Annadurai, and N. Kumar. 2024. "Exploring Novel Apalutamide Analogues as Potential Therapeutics for Prostate Cancer: Design, Molecular Docking Investigations and Molecular Dynamics Simulation." *Frontiers in Chemistry* 12, no. 1: 1418975. https://doi.org/10.3389/FCHEM.2024.1418975/BIBTEX.

Gürdal, B., and Ş. Ü. Kültür. 2013. "An Ethnobotanical Study of Medicinal Plants in Marmaris (Muğla, Turkey)." *Journal of Ethnopharmacology* 146, no. 1: 113–126. https://doi.org/10.1016/J.JEP.2012.12.012.

Guzman, J. D. 2014. "Natural Cinnamic Acids, Synthetic Derivatives and Hybrids With Antimicrobial Activity." *Molecules (Basel, Switzerland)* 19, no. 12: 19292–19349. https://doi.org/10.3390/MOLECULES191219292.

Ho, S.-T., Y.-T. Tung, Y.-L. Chen, Y.-Y. Zhao, M.-J. Chung, and J.-H. Wu. 2012. "Antioxidant Activities and Phytochemical Study of Leaf Extracts From 18 Indigenous Tree Species in Taiwan." *Evidence-Based Complementary and Alternative Medicine* 2012, no. 215959: 1–8. https://doi.org/10.1155/2012/215959.

Huang, D. W., B. T. Sherman, and R. A. Lempicki. 2009. "Systematic and Integrative Analysis of Large Gene Lists Using DAVID Bioinformatics Resources." *Nature Protocols* 4, no. 1: 44–57. https://doi.org/10.1038/nprot.2008.211.

Jo, S., T. Kim, V. G. Iyer, and W. Im. 2008. "CHARMM-GUI: A Web-Based Graphical User Interface for CHARMM." *Journal of Computational Chemistry* 29, no. 11: 1859–1865. https://doi.org/10.1002/JCC.20945.

26438429, 2025, 3, Downloaded from https://iadns.onlinelibrary.wiley.com/doi/10.1002/ffd2.545 by Turkey Cochrane Evidence Aid, Wiley Online Library on [26/10/2026]. See the Terms and Conditions (https://onlinelibrary.wiley.com/terms-and-conditions) on Wiley Online Library for rules of use; OA articles are governed by the applicable Creative Commons License

Karahan, H., D. C. Smith, B. Kim, et al. 2021. "Deletion of Abi3 Gene Locus Exacerbates Neuropathological Features of Alzheimer's Disease in a Mouse Model of Aβ Amyloidosis." *Science Advances* 7, no. 45: 1–19. https://doi.org/10.1126/SCIADV.ABE3954.

Kim, E., S. Yun Han, K. Hwang, et al. 2019. "Antioxidant and Cytoprotective Effects of (−)-Epigallocatechin-3-(3″-*O*-Methyl) Gallate." *International Journal of Molecular Science* 20, no. 16: 3993. https://doi.org/10.3390/IJMS20163993.

Kinghorn, A. D. 1994. "The Discovery of Drugs From Higher Plants." *Biotechnology (Reading, Mass.)* 26: 81–108. https://doi.org/10.1016/B978-0-7506-9003-4.50010-1.

Kurt-Celep, I., M. V. C. Nilofar, D. Zheleva-Dimitrova, et al. 2024. "From Small-Scale Studies to an Encompassing View: Inhibiting Inflammation and Clinically Relevant Enzymes With Various Extracts of *Primula vulgaris* Using In Vitro and In Silico Techniques." *Food Frontiers* 6: 329–359. https://doi.org/10.1002/FFT2.473.

Liu, F., S. Gao, Y. Yang, et al. 2017. "Curcumin Induced Autophagy Anticancer Effects on Human Lung Adenocarcinoma Cell Line A549." *Oncology Letters* 14, no. 3: 2775–2782. https://doi.org/10.3892/OL.2017.6565.

Livak, K. J., and T. D. Schmittgen. 2001. "Analysis of Relative Gene Expression Data Using Real-Time Quantitative PCR and the 2(-Delta Delta C(T)) Method." *Methods (San Diego, Calif.)* 25, no. 4: 402–408. https://doi.org/10.1006/METH.2001.1262.

Lou, Z., H. Wang, S. Zhu, C. Ma, and Z. Wang. 2011. "Antibacterial Activity and Mechanism of Action of Chlorogenic Acid." *Journal of Food Science* 76, no. 6: 398–403. https://doi.org/10.1111/J.1750-3841.2011.02213.X.

Maier, J. A., C. Martinez, K. Kasavajhala, L. Wickstrom, K. E. Hauser, and C. Simmerling. 2015. "Ff14SB: Improving the Accuracy of Protein Side Chain and Backbone Parameters From Ff99SB." *Journal of Chemical Theory and Computation* 11, no. 8: 3696–3713. https://doi.org/10.1021/ACS.JCTC.5B00255/SUPPL_FILE/CT5B00255_SI_001.PDF.

Miller, B. R., T. D. McGee, J. M. Swails, N. Homeyer, H. Gohlke, and A. E. Roitberg. 2012. "MMPBSA.Py: An Efficient Program for End-State Free Energy Calculations." *Journal of Chemical Theory and Computation* 8, no. 9: 3314–3321. https://doi.org/10.1021/CT300418H.

Nalbantsoy, A., M. Karış, L. Karakaya, and Y. Akgül. 2016. "Diyabetik Sıçanların Karaciğer Ve Böbrekleri Üzerinde Caralluma Tuberculata'nın Hipoglisemik Ve Hipolipidemik Etkisi Ve Güvenliği/*Liquidambar orientalis* Mill. Reçine Ekstraktlarının Antioksidan, Sitotoksik Ve INOS Aktiviteleri." *Turkish Journal of Biochemistry* 41, no. 3: 198–205. https://doi.org/10.1515/TJB-2016-0030.

Nunes, R., P. Pasko, M. Tyszka-Czochara, A. Szewczyk, M. Szlosarczyk, and I. S. Carvalho. 2016. "Antibacterial, Antioxidant and Anti-Proliferative Properties and Zinc Content of Five South Portugal Herbs." *Pharmaceutical Biology* 55, no. 1: 114–123. https://doi.org/10.1080/13880209.2016.1230636.

Ocsel, H., Z. Teke, M. Sacar, B. Kabay, S. Ender Duzcan, and I. G. Kara. 2012. "Effects of Oriental Sweet Gum Storax on Porcine Wound Healing." *Journal of Investigative Surgery* 25, no. 4: 262–270. https://doi.org/10.3109/08941939.2011.639847.

Okmen, G., O. Turkcan, O. Ceylan, and G. Gork. 2014. "The Antimicrobial Activity of *Liquidambar orientalis* Mill. Against Food Pathogens and Antioxidant Capacity of Leaf Extracts." *African Journal of Traditional, Complementary and Alternative Medicines* 11, no. 5: 28–33. https://doi.org/10.4314/ajtcam.v11i5.4.

Oskay, M., and D. Sarı. 2008. "Antimicrobial Screening of Some Turkish Medicinal Plants." *Pharmaceutical Biology* 45, no. 3: 176–181. https://doi.org/10.1080/13880200701213047.

Özbek, A. G., and S. E. Bilek. 2018. "Properties and Usage of *Liquidambar orientalis*." *Clinical Nutrition and Metabolism* 1, no. 5: 1–3. https://doi.org/10.15761/CNM.1000111.

Özyürek, M., K. Güçlü, and R. Apak. 2011. "The Main and Modified CUPRAC Methods of Antioxidant Measurement." *TrAC Trends in Analytical Chemistry* 30, no. 4: 652–664. https://doi.org/10.1016/J.TRAC.2010.11.016.

Perillo, B., M. Di Donato, A. Pezone, et al. 2020. "ROS in Cancer Therapy: The Bright Side of the Moon." *Experimental & Molecular Medicine* 52, no. 2: 192–203. https://doi.org/10.1038/s12276-020-0384-2.

Plumb, G. W., S. De Pascual-Teresa, C. Santos-Buelga, J. C. Rivas-Gonzalo, and G. Williamson. 2002. "Antioxidant Properties of Gallocatechin and Prodelphinidins From Pomegranate Peel." *Redox Report* 7, no. 1: 41–46. https://doi.org/10.1179/135100002125000172.

Pontiki, E., D. Hadjipavlou-Litina, K. Litinas, and G. Geromichalos. 2014. "Novel Cinnamic Acid Derivatives as Antioxidant and Anticancer Agents: Design, Synthesis and Modeling Studies." *Molecules (Basel, Switzerland)* 19, no. 7: 9655–9674. https://doi.org/10.3390/MOLECULES19079655.

Praveen, M., I. Ullah, R. Buendia, et al. 2024. "Exploring *Potentilla nepalensis* Phytoconstituents: Integrated Strategies of Network Pharmacology, Molecular Docking, Dynamic Simulations, and MMGBSA Analysis for Cancer Therapeutic Targets Discovery." *Pharmaceuticals* 17, no. 1: 134. https://doi.org/10.3390/PH17010134/S1.

Rahman, N., I. Muhammad, S. Gul Afridi, et al. 2021. "Inhibitory Effects of Plant Extracts and In Silico Screening of the Bioactive Compounds Against α-Glucosidase." *South African Journal of Botany* 143, no. 1: 330–343. https://doi.org/10.1016/J.SAJB.2020.12.002.

Rio, D. D., A. Rodriguez-Mateos, J. P. E. Spencer, M. Tognolini, G. Borges, and A. Crozier. 2013. "Dietary (Poly)Phenolics in Human Health: Structures, Bioavailability, and Evidence of Protective Effects Against Chronic Diseases." *Antioxidants & Redox Signaling* 18, no. 14: 1818–1892. https://doi.org/10.1089/ARS.2012.4581.

Rzepecka-Stojko, A., A. Kabała-Dzik, A. Moździerz, et al. 2015. "Caffeic Acid Phenethyl Ester and Ethanol Extract of Propolis Induce the Complementary Cytotoxic Effect on Triple-Negative Breast Cancer Cell Lines." *Molecules (Basel)* 20, no. 5: 9242–9262. https://doi.org/10.3390/MOLECULES20059242.

Sağdiç, O., G. Özkan, M. Özcan, and S. Özçelik. 2005. "A Study on Inhibitory Effects of Sığla Tree (*Liquidambar orientalis* Mill. Var. orientalis) Storax Against Several Bacteria." *Phytotherapy Research* 19, no. 6: 549–551. https://doi.org/10.1002/PTR.1654.

Saqallah, F. G., W. M. Hamed, W. H. Talib, R. Dianita, and H. A. Wahab. 2022. "Antimicrobial Activity and Molecular Docking Screening of Bioactive Components of *Antirrhinum majus* (Snapdragon) Aerial Parts." *Heliyon* 8, no. 8: e10391. https://doi.org/10.1016/J.HELIYON.2022.E10391.

Saraç, N., and B. Şen. 2014. "Antioxidant, Mutagenic, AntimutagenicActivities, and Phenolic Compounds of *Liquidambar orientalis* Mill. Var. Orientalis." *Industrial Crops and Products* 53, no. 17: 60–64. https://doi.org/10.1016/j.indcrop.2013.12.015.

Saravanakumar, K., C. Sarikurkcu, S. S. Sahinler, R. B. Sarikurkcu, and M. H. Wang. 2021. "Phytochemical Composition, Antioxidant, and Enzyme Inhibition Activities of Methanolic Extracts of Two Endemic Onosma Species." *Plants* 10, no. 7: 1–10. https://doi.org/10.3390/PLANTS10071373/S1.

Scheibmeir, H. D., K. Christensen, S. H. Whitaker, J. Jegaethesan, R. Clancy, and J. D. Pierce. 2005. "A Review of Free Radicals and Antioxidants for Critical Care Nurses." *Intensive & Critical Care Nursing* 21, no. 1: 24–28. https://doi.org/10.1016/J.ICCN.2004.07.007.

Slinkard, K., and V. L. Singleton. 1977. "Total Phenol Analysis: Automation and Comparison with Manual Methods." *American Journal of Enology and Viticulture* 28, no. 1: 49–55.

Sonoda, J.-I., R. Ikeda, Y. Baba, et al. 2014. "Green Tea Catechin, Epigallocatechin-3-Gallate, Attenuates the Cell Viability of Human Non-Small-Cell Lung Cancer A549 Cells via Reducing Bcl-XL Expression." *Experimental and Therapeutic Medicine* 8, no. 1: 63. https://doi.org/10.3892/ETM.2014.1719.

Thomford, N. E., D. A. Senthebane, A. Rowe, et al. 2018. "Natural Products for Drug Discovery in the 21st Century: Innovations for Novel Drug

26438429, 2025, 3, Downloaded from https://iadns.onlinelibrary.wiley.com/doi/10.1002/ffd2.545 by Turkey Cochrane Evidence Aid, Wiley Online Library on [26/10/2026]. See the Terms and Conditions (https://onlinelibrary.wiley.com/terms-and-conditions) on Wiley Online Library for rules of use; OA articles are governed by the applicable Creative Commons License

Discovery." *International Journal of Molecular Sciences* 19, no. 6: 1–29. https://doi.org/10.3390/IJMS19061578.

Treml, J., and K. Šmejkal. 2016. "Flavonoids as Potent Scavengers of Hydroxyl Radicals." *Comprehensive Reviews in Food Science and Food Safety* 15, no. 4: 720–738. https://doi.org/10.1111/1541-4337.12204.

Trott, O., and A. J. Olson. 2010. "AutoDock Vina: Improving the Speed and Accuracy of Docking With a New Scoring Function, Efficient Optimization and Multithreading." *Journal of Computational Chemistry* 31, no. 2: 461. https://doi.org/10.1002/JCC.21334.

Tsai, C.-M., G.-C. Yen, F.-M. Sun, S.-F. Yang, and W. Chia-Jui. 2013. "Assessment of the Anti-Invasion Potential and Mechanism of Select Cinnamic Acid Derivatives on Human Lung Adenocarcinoma Cells." *Molecular Pharmaceutics* 10, no. 5: 1890–1900. https://doi.org/10.1021/MP3006648.

Ulusoy, H., Ş. Ceylan, and H. Peker. 2021. "Determination of Antioxidant and Antimicrobial Activity of Sweetgum (*Liquidambar orientalis*) Leaf, a Medicinal Plant." *Polímeros* 31, no. 2: 1–7. https://doi.org/10.1590/0104-1428.04221.

Valdés-Tresanco, M. S., M. E. Valdés-Tresanco, P. A. Valiente, and E. Moreno. 2021. "Gmx_MMPBSA: A New Tool to Perform End-State Free Energy Calculations With GROMACS." *Journal of Chemical Theory and Computation* 17, no. 10: 6281–6291. https://doi.org/10.1021/ACS.JCTC.1C00645.

Yagi, S., G. Zengin, O. A. Eldahshan, et al. 2024. "Functional Constituents of *Colchicum lingulatum* Boiss. & Spruner Subsp. *Rigescens* K. Perss. Extracts and Their Biological Activities With Different Perspectives." *Food Bioscience* 60, no. 1: 104496. https://doi.org/10.1016/J.FBIO.2024.104496.

Zengin, G., and A. Aktumsek. 2014. "Investigation of Antioxidant Potentials of Solvent Extracts From Different Anatomical Parts of *Asphodeline anatolica* E. Tuzlaci: An Endemic Plant to Turkey." *African Journal of Traditional, Complementary, and Alternative Medicines: AJTCAM* 11, no. 2: 481–488. https://doi.org/10.4314/AJTCAM.V11I2.37.

Zengin, G., L. Menghini, L. Malatesta, et al. 2016. "Comparative Study of Biological Activities and Multicomponent Pattern of Two Wild Turkish Species: *Asphodeline anatolica* and *Potentilla speciosa*." *Journal of Enzyme Inhibition and Medicinal Chemistry* 31, no. 1: 203–208. https://doi.org/10.1080/14756366.2016.1178247.

Zengin, G., A. Uysal, A. Diuzheva, et al. 2018. "Characterization of Phytochemical Components of *Ferula halophila* Extracts Using HPLC-MS/MS and Their Pharmacological Potentials: A Multi-Functional Insight." *Journal of Pharmaceutical and Biomedical Analysis* 160, no. 1: 374–382. https://doi.org/10.1016/J.JPBA.2018.08.020.

Zengin, G., M. Veysi Cetiz, N. Abul, et al. 2024. "Establishing a Link Between the Chemical Composition and Biological Activities of *Gladiolus italicus* Mill. From the Turkish Flora Utilizing In Vitro, In Silico and Network Pharmacological Methodologies." *Toxicology Mechanisms and Methods* 1–21. https://doi.org/10.1080/15376516.2024.2397387.

Zhang, J., S. Xue, H. Chen, et al. 2024. "Exploring the Mechanism of Si-Miao-Yong-an Decoction in the Treatment of Coronary Heart Disease Based on Network Pharmacology and Experimental Verification." *Combinatorial Chemistry & High Throughput Screening* 27, no. 1: 57–68. https://doi.org/10.2174/1386207326666230703150803.

Zhu, X., R. Li, C. Wang, et al. 2021. "Pinocembrin Inhibits the Proliferation and Metastasis of Breast Cancer Via Suppression of the PI3K/AKT Signaling Pathway." *Frontiers in Oncology* 0: 2804. https://doi.org/10.3389/FONC.2021.661184.

Supporting Information

Additional supporting information can be found online in the Supporting Information section.

26438429, 2025, 3, Downloaded from https://iadns.onlinelibrary.wiley.com/doi/10.1002/ffd2.545 by Turkey Cochrane Evidence Aid, Wiley Online Library on [26/10/2026]. See the Terms and Conditions (https://onlinelibrary.wiley.com/terms-and-conditions) on Wiley Online Library for rules of use; OA articles are governed by the applicable Creative Commons License